JNC TY9400 2004-009

粒子法を用いたNa-水反応時の流動様式評価に関する研究

― 混相流における粒子法を用いた液滴分裂挙動および流動様式の数値解析 ―

先行基礎工学研究分野に関する最終詳細報告書

（共同研究報告書）

２００４年７月

東　京　大　学
核燃料サイクル開発機構
大洗工学センター

〒319-1184　茨城県那珂郡東海村村松4番地49
核燃料サイクル開発機構
技術展開部　技術協力課
電話：029-282-1122（代表）
ファックス：029-282-7980
電子メール：jserv@jnc.go.jp

Ⓐ

JNC TY9400 2004-009
2004年 7月

粒子法を用いたNa-水反応時の流動様式評価に関する研究
－混相流における粒子法を用いた液滴分裂挙動および流動様式の数値解析－

先行基礎工学分野に関する最終詳細報告書（共同研究報告書）

段　日強[1]、越塚　誠一[1]
高田　孝[2]、山口　彰[2]

要旨

ナトリウム冷却高速増殖炉における蒸気発生器伝熱管破損事故は、ナトリウム-水反応に伴い周囲伝熱管への副次的損傷拡大の可能性があるため、安全評価上重要である。その伝熱流動現象の解明には、混相流における流動様式や界面面積などの知見が重要である。本研究では粒子法を用いた機構論的な数値解析により、混相流における流動様式および界面面積の評価に関する研究を平成14年度より２ヶ年にわたって実施した。

粒子法では格子を一切使用しないことから、流体の分裂や合体を扱うことが容易である。蒸気発生器伝熱管破損事故では、高温高圧の水が低圧のナトリウム中に噴出するので、噴出ジェットの分裂およびさらに細かい液滴への分裂（粒子ブレークアップ）が生じる。したがって、粒子法はこうした現象の解析に適している。

本共同研究より得られた主な成果を以下に示す。

・粒子ブレークアップの数値計算をおこない、液滴分裂のメカニズムを解明するとともに、臨界ウエーバー数を導出した。
・水の急速沸騰のモデル化をおこない、液体ナトリウム中に水が噴出する計算をおこなった。
・上記計算結果と臨界ウエーバー数に基づき界面面積を評価した。

[1]東京大学　大学院工学系研究科　システム量子工学専攻
[2]核燃料サイクル開発機構　大洗工学センター 要素技術開発部 流体計算工学研究グループ

JNC TY9400 2004-009
July, 2004

Numerical Simulation of Multi-Phase Flow in Sodium-Water Reaction using MPS Method
- Numerical Investigation of Droplet Breakup and Flow Regime -
(Final report of the JNC cooperative research scheme on the nuclear fuel cycle)

Duan Ri-Oiang[1], Koshizuka Seiichi[1]
Takata Takashi[2], Yamaguchi Akira[2]

Abstract

Tube rupture accidents in steam generators of sodium-cooled fast breeder reactors are important for safety because the rupture may propagates to neighboring tubes due to sodium-water reaction. In order to clarify the thermal-hydraulic phenomena in the accidents, the flow pattern and the interface in multi-phase flow must be investigated. The JNC cooperative research scheme on the nuclear fuel cycle with The University of Tokyo has been carried out to investigate a flow regime and interfacial area density of multi-phase flow in sodium-water reaction using the Moving-Particle Semi-implicit (MPS) method. Since grids are not necessary in the MPS methods, it is not difficult to analyze separation and merging of fluids. In the tube rupture accidents in steam generators, high-pressure and high-temperature water is discharged into low-pressure sodium. Discharged water is disintegrated from a jet to droplets and further disintegrated to smaller droplets (droplet breakup). Thus, the MPS method is fitted to these phenomena.

The following conclusions were obtained in this research.

- Numerical analysis of the droplet breakup process was carried out. Breakup mechanisms was clarified and the critical Weber number was obtained.
- Water flashing was modeled for the particle method and numerical simulation of water discharge into sodium was analyzed.
- The interfacial area was evaluated based on the above results.

[1] Department of Quantum Engineering and Systems Science, School of Engineering,
The University of Tokyo

[2] Thermal-Hydraulic Research Group, Advanced Technology Division,
O-arai Engineering Center, JNC

Contents

Table Contents

【Chapter 3】

Figure Contents

【Chapter 2】

【Chapter 3】

【Chapter 4】

1. Introduction

Tube rupture accidents in steam generators of sodium-cooled fast breeder reactors are important for safety because the rupture may propagates to neighboring tubes due to sodium-water reaction. The steam generators must be designed to avoid the propagation of the tube rupture. On the other hand, economical design is required to commercialize the fast breeder reactors, which means that components, involving the steam generators, are to be compact as possible. Therefore, sophisticated technologies must be developed to meet both safety and economical requirements. First of all, we need to clarify the thermal-hydraulic phenomena of sodium-water reaction accidents.

In the tube rupture accidents in the steam generators, water, sodium, steam and hydrogen are main components of the thermal-hydraulics. Steam is generated by the phase change from water. Hydrogen is generated by the sodium-water reaction. These materials make multi-phase flow of two liquid components and two gas components. Sodium-water reaction will be governed by the interfacial area between sodium and water, and sodium and steam. If the interfacial area is large, the reaction is rapid. We need to determine the interfacial area to predict the sodium-water reaction. However, in multi-phase flow, there exist many flow patterns, such as bubbly, slag, droplet, etc. The interfacial area depends on the flow pattern. The flow pattern and the interface are in multi-phase flow must be investigated.

In the present study, the flow pattern and the interface area in multi-phase flow are evaluated by mechanistic numerical analysis using a particle method. MPS (Moving Particle Semi-implicit) method is used. The MPS method was developed by the present

authors [1-1, 1-2]. Governing equations are transformed to particle interactions without grids. Wave breaking, which involves complex motion of free surfaces, was successfully analyzed by the MPS method [1-3]. Since grids are not necessary in the particle methods, it is not difficult to analyze separation and merging of fluids. Phase change model was also developed and multi-phase flow was calculated [1-4]. In the tube rupture accidents in steam generators, high-pressure and high-temperature water is discharged into low-pressure sodium. Discharged water is disintegrated from a jet to droplets and further disintegrated to smaller droplets (droplet breakup). Thus, the particle method is fitted to these phenomena.

In this paper, the following studies are provided. First, numerical analysis of the droplet breakup process is carried out. Breakup mechanisms is clarified and the critical Weber number is obtained. Secondly, water flashing is modeled for the particle method and numerical simulation of water discharge into sodium is analyzed. Thirdly, the interfacial area is evaluated based on the above results. The fundamental knowledge is acquired in this study. This will be useful in the more macroscopic and practical codes which have been developed in JNC [1-5].

References

1-1) S. Koshizuka, H. Tamako and Y. Oka, "A Particle Method for Incompressible Viscous Flow with Fluid Fragmentation," Comput. Fluid Dynamics J. 4, 29-46 (1995)

1-2) S. Koshizuka and Y. Oka, "Moving-Particle Semi-implicit Method for Fragmentation of Incompressible Fluid," Nucl. Sci. Eng. 123, 421-434 (1996)

1-3) S. Koshizuka, A. Nobe and Y. Oka, "Numerical Analysis of Breaking Waves Using the Moving Particle Semi-implicit Method," Int. J. Numer. Meth. Fluids 26, 751-769 (1998)

1-4) S. Koshizuka, H. Ikeda and Y. Oka, "Numerical Analysis of Fragmentation Mechanisms in Vapor Explosions," Nucl. Eng. Des. 189, 423-433 (1999)

1-5) T. Takata, A. Yamaguchi and A. Watanabe, "Modification of Multi-dimensional Sodium-Water Reaction Analysis Code: SERAPHIM and Sensitivity Analyses on the Early Stage of Leakage," JNC TN9400 2003-024 (2003)

2. Critical Weber Number of Droplet Breakup

2.1 Introduction

A droplet is subject to breakup under an impulsive acceleration in another continuous fluid, which is a fundamental process in many industrial and natural phenomena. Experimental observations show that there are five distinct regimes of droplet breakup, i.e. vibration, bag, bag-and-stamen, sheet stripping, and explosive. Hinze [2-1)] had shown that transitions between breakup regimes are largely dependent on the Weber number, $\mathrm{We} = \rho_c D_0 U_0^2 / \sigma$, and the Ohnesorge number, $\mathrm{On} = \mu_d / (\rho_d D_0 \sigma)^{1/2}$, where the subscript *c, d,* and *o* represent respectively the continuous phase, the droplet phase, and the initial state. The Weber number stands for the ratio of disruptive hydrodynamic force to stabilizing force; and the Ohnesorge number reflects the effect of droplet viscosity on droplet breakup. The critical Weber number (thereafter, $\mathbf{We_{cr}}$) is defined as the value at which droplet breakup occurs. Generally, the interphasic transfer of momentum, heat, and the chemical reaction rate are proportional to the interfacial area, which is correlated with $\mathbf{We_{cr}}$. In safety analyses of nuclear reactors, the evaluation of the severity of the accidents, i.e. the two typical cases such as water-to-sodium leak in steam generators of fast breeder reactors and fuel-coolant interaction in light water reactors, is involved with $\mathbf{We_{cr}}$ of droplet breakup.

Dimensional analyses indicate that there are three independent dimensionless parameters affecting $\mathbf{We_{cr}}$ for a droplet subjected to an impulsive acceleration. From physical viewpoints, they are conventionally expressed by the Reynolds number

associated with continuous fluid properties, the Ohnesorge number and the density ratio of droplet to continuous fluid [2-2)]. The dependences on the two former parameters had been paid much attention to by previous researchers, and such reviews were comprehensively made by Pilch & Erdman [2-3)], Kolev [2-4)] and Gelfand [2-5)]. However, knowledge on the effect of density ratio on $\mathbf{We_{cr}}$ is limited.

Experimental observations indicate that there are three mechanisms of droplet breakup, namely, droplet deformation, boundary-layer stripping, and surface disturbances caused by the Kelvin-Helmholtz (thereafter, K-H) and Rayleigh-Taylor (thereafter, R-T) instabilities [2-5)]. In fact, the above three mechanisms coexist in parallel for droplet breakup. Definitely, density ratio has great effect on $\mathbf{We_{cr}}$ from the viewpoint of surface disturbances. The K-H instability is a consequence of the relative tangential motion of two phases at the phase-dividing interface. The R-T instability is caused by the inertia of the denser fluid when the system experiences an acceleration perpendicular to the interface in direction of the denser fluid. In the following, we use the method of normal mode to analyze linear region of the K-H and R-T instabilities for droplet breakup, inducing roughly the effect of density ratio on $\mathbf{We_{cr}}$.

For the K-H instability, an interfacial disturbance ϕ satisfies the Laplace's equation.

$$\nabla^2 \phi = 0 \tag{2-1}$$

Assuming a normal mode solution for ϕ is as follows:

$$\phi(x,t) = \phi_0 e^{i(k \cdot x - \omega t)} \tag{2-2}$$

where k is its wave number of the disturbance, and ω is its angular frequency. The dispersion relation (exponential growth rate) of the disturbance in linear region is given as:

$$\omega = k\left(\frac{\rho_c U_c + \rho_d U_d}{\rho_c + \rho_d} \pm \frac{\sqrt{(\rho_c + \rho_d)k\sigma - \rho_c \rho_d (U_c - U_d)^2}}{\rho_c + \rho_d} \right) \tag{2-3}$$

The critical wave number, k_{cr}, and critical wavelength, λ_{cr}, for this disturbance are:

$$k_{cr} = \frac{\rho_c \rho_d (U_c - U_d)^2}{\sigma(\rho_c + \rho_d)} \tag{2-4}$$

$$\lambda_{cr} = \frac{2\pi}{k_{cr}} = \frac{2\pi\sigma(\rho_c + \rho_d)}{\rho_c \rho_d (U_c - U_d)^2} \tag{2-5}$$

Brodkey [2-6] indicated that the critical radius of a droplet for breakup is the largest radius that is stable when the droplet is subjected to a small disturbance. So $\mathbf{We_{cr}}$ can be determined by setting the radius of a droplet equal to the critical wavelength, $D_0/2 = \lambda_{cr}$.

$$\mathrm{We}_{cr} = \frac{\rho_c (U_c - U_d)^2 D_0}{\sigma} = 4\pi\left(1 + \frac{\rho_c}{\rho_d}\right) = 4\pi\left(1 + \frac{1}{s}\right) \tag{2-6}$$

where $s = \rho_d / \rho_c$, is the density ratio of the droplet to continuous phase. The dependence of $\mathbf{We_{cr}}$ on density ratio from Eq.(2-6) is shown in Fig.2-1.

Similar analysis as the above for the R-T instability performed is shown in the following. Neglecting the viscosity effect, the dispersion relation of a disturbance for two uniform fluids with different density under certain acceleration is as follows:

$$\omega = \left(\frac{ka(\rho_d - \rho_c)}{\rho_d + \rho_c} - \frac{\sigma k^3}{\rho_d + \rho_c} \right)^{1/2} \tag{2-7}$$

where, a is the acceleration in direction from phase d to phase c, assuming $\rho_d > \rho_c$. The critical wavelength, λ_{cr}, for the disturbance is given:

$$\lambda_{cr} = 2\pi \left(\frac{\sigma}{a(\rho_d - \rho_c)} \right)^{1/2} \tag{2-8}$$

Setting the radius of a droplet equal to the critical wavelength, $D_0/2 = \lambda_{cr}$, the critical Weber number is obtained as:

$$\mathrm{We}_{cr} = 4\pi (U_c - U_d)^2 \sqrt{\frac{\rho_c}{a\sigma(s-1)}} = C\sqrt{\frac{1}{s-1}} \tag{2-9}$$

Assuming all parameters but density ratio in Eq. (2-9) being constant, the dependence of $\mathbf{We_{cr}}$ on density ratio for the R-T instability is shown in Fig.2-2.

The above linear analyses reveal that $\mathbf{We_{cr}}$ is inversely proportional to density ratio. Of course, the other two mechanisms also make contribution to the effect of density ratio.

In this chapter, we use the Moving Particle Semi-implicit (thereafter, MPS) method [2-7] to investigate the effect of density ratio on $\mathbf{We_{cr}}$. The MPS method has advantages to treat such fluid flows as with large deformation, irregularity of geometry and multi-fluid flows [2-8, 2-9]. The rest of the chapter is organized as follows. The description of the MPS method and surface tension model is given in Section 2. In Section 3, we present the numerical simulation of droplet breakup. In Section 4 and Section 5, the critical

Weber number and the breakup Weber number (its definition seen later) at different density ratios are investigated. Our conclusions appear in Section 6.

2.2 Numerical models

The MPS method is based on fully Lagrangian description. Fluid is represented by particles. Numerical diffusion does not arise because the convection terms are not discretized. Differential operators in the governing equations, such as gradient, divergence and Laplacian operator, are transformed to equivalent particle interactions using a weight function. Grids are not necessary. Large deformation of interface can be analyzed without grid tangling. A semi-implicit algorithm is employed for incompressible flows. The incompressibility constraint is implicitly satisfied by solving a Poisson equation of pressure, while the other terms in momentum equations are explicitly calculated.

2.2.1 governing equations

The mass and momentum conservation equations of incompressible flows are as follows:

$$\frac{D\rho}{Dt} = 0 \tag{2-10}$$

$$\rho \frac{D\mathrm{u}}{Dt} = -\nabla P + \mu \nabla^2 \mathrm{u} + \rho \mathrm{g} + \sigma \kappa \delta(s) \mathrm{n}_s \tag{2-11}$$

where *D/Dt* denotes the Lagrangian derivative involving convection terms, ρ and μ are the density and viscosity respectively, g is the acceleration of gravity, σ is the

interfacial tension, κ is the mean curvature of interface, $\delta(s)$ is the Dirac delta function concentrated on interface, and $\mathbf{n}_s$ is the unit normal vector to interface.

2.2.2 particle interaction models

In the MPS method, the differential operators in the governing equations are modeled by particle interactions, which are limited among neighboring particles covered with a weight function:

$$w(r)=\begin{cases}\dfrac{r_e}{r}-1 & 0\le r<r_e \\ 0 & r_e\le r\end{cases} \qquad (2\text{-}12)$$

where r_e is the radius of the interaction area (taken as 2 l_0, l_0 represents the distance between two adjacent particles in the initial arrangement); and r is the distance between two particles. Summation of the weight functions is called particle number density, n_i, which is used as a normalization factor for averaging.

$$n_i=\sum_{j\neq i} w\left(\left|\mathbf{r}_j-\mathbf{r}_i\right|\right). \qquad (2\text{-}13)$$

The particle number density represents its fluid density. It should be constant for incompressible flows: $n_i=n^0$, where n^0 is dependent on the initial arrangement of particles.

The gradient and Laplacian operator in the governing equations are transformed to equivalent particle interactions. If Φ is an arbitrary scalar, particle interaction models for differential operators are expressed as

$$\left\langle \nabla \Phi \right\rangle_i = \frac{d}{n^0} \sum_{j \neq i} \left[\frac{\Phi_j - \Phi_i}{\left| \mathbf{r}_j - \mathbf{r}_i \right|^2} (\mathbf{r}_j - \mathbf{r}_i) w\left(\left| \mathbf{r}_j - \mathbf{r}_i \right| \right) \right] \tag{2-14}$$

$$\left\langle \nabla^2 \Phi \right\rangle_i = \frac{2d}{\zeta_i n^0} \sum_{j \neq i} \left[(\Phi_j - \Phi_i) w\left(\left| \mathbf{r}_j - \mathbf{r}_i \right| \right) \right] \tag{2-15}$$

where d is the number of space dimension and ζ_i is defined as

$$\zeta_i = \frac{\sum_{j \neq i} \left| \mathbf{r}_j - \mathbf{r}_i \right|^2 w\left(\left| \mathbf{r}_j - \mathbf{r}_i \right| \right)}{\sum_{j \neq i} w\left(\left| \mathbf{r}_j - \mathbf{r}_i \right| \right)} \tag{2-16}$$

The gradient model, Eq. (2-14), is obtained as the average of gradient vectors that are determined between the ith particle and its neighborings. The Laplacian operator model, Eq. (2-15), is derived from the physical concept of diffusion. Parameter ζ_i is introduced to keep the same variance increase as that of the analytical solution. Substituting the above particle interaction models into the governing equations, we can obtain the particle dynamics to simulate fluid flows. More detail is described in the reference [2-7].

2.2.3 computational algorithm

A semi-implicit algorithm is used for incompressible flows in the MPS method. For incompressible flows, the continuity equation requires that fluid density be kept constant. This is equivalent to hold particle number density n_i being constant. In each time step, the governing equations are calculated through two stages.

In the first stage, all terms in the momentum conservation equations except for the pressure gradient term are explicitly calculated and the temporal velocities and positions of particles are obtained:

$$\mathbf{u}_i^* = \mathbf{u}_i^n + \Delta t\left(\upsilon\nabla^2\mathbf{u}^n + \mathbf{g} + \sigma\kappa\delta(s)\mathbf{n}_s/\rho_i\right), \tag{2-17}$$

$$\mathbf{r}_i^* = \mathbf{r}_i^n + \Delta t \cdot \mathbf{u}_i^* \tag{2-18}$$

where υ is the kinematical viscosity. However, the incompressibility constraint may not be satisfied, that is to say, the temporal particle number density n^* is not n^0. So the temporal value n^* should be implicitly corrected to n^0 by

$$n' = n^0 - n^* \tag{2-19}$$

where n' is the correction value, which is related to the velocity correction $\mathbf{u}'$ through the mass conservation equation:

$$\frac{1}{\Delta t}\frac{n'}{n^0} = -\nabla \cdot \mathbf{u}' \tag{2-20}$$

The velocity correction is derived from the implicit pressure gradient term as

$$\mathbf{u}' = -\frac{\Delta t}{\rho}\nabla P^{n+1} \tag{2-21}$$

With Eqs.(2-19)~(2-21), a Poisson equation of pressure is obtained:

$$\nabla^2 P_i^{n+1} = -\frac{\rho}{\Delta t^2}\frac{n^*{}_i - n^0}{n^0} \tag{2-22}$$

In the second stage, the above Poisson equation of pressure is solved by the Incomplete Cholesky Preconditioning Conjugate Gradient (ICCG) method. Then the velocities and the positions of particles are modified by pressure gradient.

2.2.4 surface tension model

Surface tension is computed at the particles that lie on interface [2-10)]. We use the particle number density, n^{st}, relative to the droplet phase (i.e. excluding the contribution

of continuous phase) to catch interface. The constant, n_0^{st}, is correspondent to interior particles of the droplet for incompressibility constraint. When a particle whose particle number density satisfies

$$n_*^{st} < \beta n_0^{st} \tag{2-23}$$

is regarded as an interfacial particle, where β is a parameter below 1, herein taken as β=0.97. Such particles occupy a d^{st} thickness region. Koshizuka & Oka [2-6)] had shown that computational results are not sensitive to the value of β.

The surface tension model is shown in Fig.2-3. The curvature κ and the unit normal vector **n** of interfacial particles are calculated also based on particle number density, however its weight function is different from Eq. (2-12). The procedure of calculating the curvature κ is as follows.

Firstly, recalculating a particle number density of interfacial particles:

$$n_i^{st1} = \sum_{j \neq i} w_i^{st1}\left(\left|\mathrm{r}_j - \mathrm{r}_i\right|\right) \tag{2-24}$$

the above weight function is defined as:

$$w_i^{st1}\left(\left|\mathrm{r}_j - \mathrm{r}_i\right|\right) = \begin{cases} 1 & 0 \le \left|\mathrm{r}_j - \mathrm{r}_i\right| < r_e^{st} \\ 0 & r_e^{st} \le \left|\mathrm{r}_j - \mathrm{r}_i\right| \end{cases} \tag{2-25}$$

where r_e^{st} is taken as $3.1 l_0$ in this study. It was found that the particle number density, n_i^{st1}, increases along the direction pointed to the interior of the droplet in the d^{st} thickness region. This leads to errors for the curvature calculation.

So in the second step, a new particle number density for the interfacial particles is calculated again based on another weight function. It is shown as follows.

$$n_i^{st2} = \sum_{j \neq i} w_i^{st2}\left(\left|\mathrm{r}_j - \mathrm{r}_i\right|\right) \tag{2-26}$$

this weight function is defined as:

$$w_i^{st2}\left(\left|\mathrm{r}_j - \mathrm{r}_i\right|\right) = \begin{cases} 1 & 0 \le \left|\mathrm{r}_j - \mathrm{r}_i\right| < r_e^{st} \quad \text{and} \quad n_j^{st1} > n_i^{st1} \\ 0 & \text{otherwise} \end{cases} \tag{2-27}$$

The angle θ between the tangent directions at the *i*th and *j*th interfacial particles (their distance is r_e^{st}) is proportional to the particle number density n_i^{st2}.

$$2\theta = \frac{n_i^{st2}}{n_0^{st1}}\pi \tag{2-28}$$

where n_0^{st1} corresponds to that an interface is a plane, which is equal to half of the particle number density of an interior particle of droplet. Since the curvature κ is the derivative of the unit tangent vector t with respect to the arc length *l*, it is calculated as:

$$\kappa = \left|\frac{d\mathsf{t}}{dl}\right| = \frac{2\cos\theta}{r_e^{st}} \tag{2-29}$$

The unit normal vector is also calculated through particle number density, whose weight function is taken as Eq. (2-25). The particle number densities at four positions near the *i*th particle are evaluated, $n_i^{\pm x}(\mathbf{r}_i \pm l_0\mathbf{n}_x)$and $n_i^{\pm y}(\mathbf{r}_i \pm l_0\mathbf{n}_y)$. The unit normal vector to the interface is calculated by:

$$\mathsf{a}_i = \frac{n_i^{+x} - n_i^{-x}}{2l_0}\mathsf{n}_x + \frac{n_i^{+y} - n_i^{-y}}{2l_0}\mathsf{n}_y \tag{2-30}$$

$$\mathbf{n}_i = \frac{\mathbf{a}_i}{|\mathbf{a}_i|} \tag{2-31}$$

where vectors $\mathbf{n}_x$ and $\mathbf{n}_y$ are the unit vectors in *x*- and *y*-direction, respectively.

The above surface tension model is verified by oscillation of a square ethanol droplet due to surface tension. Its dimension is 3×3 mm, density ρ=797.88 kg/m^3 and surface tension coefficient σ=0.02361 N/m. According to the Rayleigh linear theory for a small amplitude oscillation of a cylindrical droplet, the theoretical oscillation period is *t*=0.0328 s for the above droplet [2-11)]. The numerical simulation of its evolution under surface tension is shown in Fig.2-4. Its oscillation period is about 0.033 s, which is in agreement with the theoretical value.

2.3 Numerical simulation of droplet breakup

Two-dimensional numerical simulations are conducted. The computational configuration is illustrated in Fig.2-5. The following shown is a example case, which corresponds to a uranium dioxide droplet in water. The properties of droplet and water are as: the initial diameter of the droplet is 0.009m, its density 9000 kg/m^3, its viscosity 2.82×10^{-4} Pa·Sec., and its surface tension 0.4 N/m, and the density of water 1000 kg/m^3. The total number of particles is 8115, 256 of which represents the droplet.

In the following Figs.2-6~2-8, the upper numbers under the figures indicate absolute time ***t*** (s, except for Fig.2-8 in μs), which starts from the moment when continuous fluid begins to pass over the droplet, the lower numbers give the value of dimensionless time $\tau = t\,\tau_0^{-1}$, where $\tau_0 = D_0 / U_0 \sqrt{\rho_c / \rho_d}$ is the chosen characteristic time scale. The evolutions of droplet shape under impulsive acceleration obtained from

computational simulations respectively at **We**=12 and 13 are shown in Figs.2-6 and 2-7, whereof in Fig.2-7 the so-called vibration regime of breakup is illustrated. The vibration regime of breakup is characterized by progressing deformation and subsequent droplet breakup into two or more fragments. Comparing realistic three-dimensional investigations, the two-dimensional droplet has a lower translation velocity due to the larger pressure drag for circular cylinder than circular sphere. From the viewpoint of deformation mechanism of droplet breakup, there are qualitative similarity of pressure distribution and surface tension for circular cylinder and sphere. And from the viewpoint of hydrodynamic instabilities, the coherent vortical structures behave different in two dimension with respect to three dimension; but as Zaleski, etc. [2-12] pointed out, this may just affect smallest scales of vortex for a large Weber breakup. So the two dimensional simulation may be qualitatively compared to experimental results[2-13]. The experimental observations of vibration regime breakup of droplet by Gelfand [2-5] are shown in Fig.2-8. And the dimensionless time of breakup shown in Fig.2-7 is also within the range, $\tau \approx 2.8 \sim 4$, of experimental data for the vibration breakup mode [2-5].

From the above simulation results, two observations are obtained. Firstly, droplet breakup does not occur below **We**=13 for a uranium dioxide droplet in water; so $\mathbf{We_{cr}}$ is approximate to 13, which is close to the experimental value ($\mathbf{We_{cr}}$=17) for a mercury droplet breakup in water [2-14]. Secondly, the co-action of pressure drag and surface tension on a droplet is easily explained in Fig.2-6. Under an impulsive acceleration, a droplet is first deformed due to the asymmetric distribution of pressure on the bow and stern of the droplet. However, the relative motion between the droplet and continuous fluid is gradually decreased due to flow resistance. As pressure drag is insufficient to

overcome surface tension force, the droplet would recover to its original shape with a small amplitude oscillation.

2.4 Effect of density ratio on We_{cr}

The following density ratios were investigated, $s=\rho_d/\rho_c$ =1, 3, 5, 7 and 9. The initial Reynolds number, $\mathrm{Re}=U_0 D_0 \rho_c/\mu_c$, is constantly kept 650 by fixing the continuous phase viscosity, density, initial velocity of droplet, and the initial droplet diameter. The Ohnesorge number is kept about 4.15×10^{-5} by adjusting the droplet viscosity and surface tension. The dependence of $\mathbf{We_{cr}}$ on density ratio from the MPS method is illustrated in Fig.2-9, where the square marks represent the computational results, and the solid line is the fitting curve of the computational results by the least square method on power function. The resultant fitting equation is obtained

$$We_{cr} = 64.36\, s^{-0.82} \tag{2-32}$$

Due to simplification of a spherical droplet to a two-dimensional cylindrical droplet in the above simulations, somewhat discrepancy of $\mathbf{We_{cr}}$ with the actual situations maybe exists for the value of $\mathbf{We_{cr}}$ at a specific density ratio. In the view of mechanical action on a droplet, pressure drag acting on a sphere would be smaller than that acting on a cylinder with an identical diameter at same flow conditions; however, surface tension force on a sphere would be larger than that on a cylinder because one of the two principal radii of curvatures (as R_1 and R_2) is infinite for a cylinder and hereby taken $R_2=\infty$, as shown in the following equations.

$$p_\sigma = \sigma\left(\frac{1}{R_1}+\frac{1}{R_2}\right) = \sigma\left(\frac{1}{R_1}+\frac{1}{\infty}\right) = \sigma\frac{1}{R_1} \qquad \text{for circular cylinder;}$$

$$p_\sigma = \sigma\left(\frac{1}{R_1}+\frac{1}{R_2}\right) = 2\sigma\frac{1}{R_1} \qquad \text{for sphere.}$$

Therefore the values of $\mathbf{We_{cr}}$ for a sphere droplet would be somewhat higher than the above computational values at correspondent density ratios. But the trend of the dependence of $\mathbf{We_{cr}}$ on density ratio should be similar for spherical and cylindrical droplets.

The computational results indicate that $\mathbf{We_{cr}}$ is inversely proportional to density ratio, and specifically $\mathbf{We_{cr}}$ is strongly dominated by density ratio as it is less than 3, but weakly decreased as it is greater that 3. In the view of the trend of dependence of $\mathbf{We_{cr}}$ on density ratio, agreement with the linear analyses of surface disturbances is quite satisfying. And moreover, these results also agree with the nonlinear analysis of Kelvi-Helmholtz instability for large amplitudes of disturbances. Rangel and Sirignano [2-15)] investigated the density ratio effects on the nonlinear growth of the K-H instability using the vortex-discretization method. They showed that the wavelength spectrum of surface disturbances is divided into a region where a vorticity singularity develops with interface rollup and a region where a vorticity singularity does not develop with partial or no rollup. The transition occurs at decreasing value of a wavelength (equivalently, the Weber number) for large density difference. At large enough values of density difference, this transition becomes less evident because the surface tension plays a decreasingly important role as the stabilizing agent for this large density difference.

2.5 Breakup Weber number

2.5.1 centroid velocity of a droplet before onset of breakup

The centroid velocity, $\overline{U}$, of a droplet is defined as the average of the velocities, U_i, of all droplet particles, i.e. $\overline{U} = \sum_i^{Nd} U_i$, where N_d is the total particle number representative of the droplet. Pilch & Erdman [2-3)] reviewed the experimental data on droplet velocity and proposed the following empirical correlation on the centroid velocity of droplet for liquid-liquid systems.

$$\overline{U} = \left(1 - \frac{0.75 C_D T}{s^{0.5} + 0.75 C_D T}\right) U_0 \qquad (2\text{-}33)$$

where U_0 is the initial centroid velocity, s is the density ratio s= ρ_d / ρ_c , C_D is the effective drag coefficient, C_D=2.5~3.0 for liquid-liquid systems, and T is the dimensionless time, which definition is as follows:

$$T = t \frac{U_0}{d_0 s^{0.5}} \qquad (2\text{-}34)$$

where t is the absolute time.

The evolution of the centroid velocity of droplet is compared with the above empirical correlation (2-33). They agree well. Figure 2-10 shows the centroid velocity with dimensionless time for **We**=17 and density ratio=5 as a demonstrative case.

2.5.2 breakup Weber number

Breakup Weber number is defined as $\mathrm{We_{br}} = \rho_c D_0 \overline{U}_{br}^2 / \sigma$, where $\overline{U}_{br}$ is the centroid velocity of droplet at the instant of breakup onset. The dependence of the breakup Weber number on density ratio is shown in Fig.2-11, which shows that the

breakup Weber number is almost constant and close to 0.4, which is little dependent on density ratio.

From the viewpoint of physics, $\mathbf{We_{br}}$ stands for restoring force for resisting droplet breakup, and is correspondent with minimum disruptive force that should be required before droplet breakup. It can be theoretically assumed that if the relative velocity between a droplet and another continuous fluid, whose Weber number is the breakup Weber number, is kept constant, the droplet eventually would experience breakup. It should be noted that $\mathbf{We_{cr}}$ reflects the minimum requirement of initial inertial force to make droplet breakup at a certain restoring force under an impulsive acceleration. Due to the fact that the restoring force, viz. surface tension, is an inherent force for droplet, $\mathbf{We_{br}}$ is just associated with the droplet itself, and little dependent on density ratio of droplet to continuous fluid. However, the occurrence of droplet breakup is the consequence of competition of exterior disruptive force with the inherent restoring force. So $\mathbf{We_{cr}}$ is associated with both droplet and continuous fluid, and higher than $\mathbf{We_{br}}$ due to decreasing disruptive force with time caused by flow resistance.

2.6 Conclusions

The effect of density ratio on the critical Weber number has been studied for droplet breakup for liquid-liquid systems by numerical simulations and theoretical analyses. The investigated range of density ratio covers hydrodynamic safety accidents occurred in nuclear reactors. The results show that the critical Weber number is inversely proportional to density ratio; and specifically the critical Weber number is a strong function with density ratio as it is less than 3, but weakly decreased as it is

greater than 3. Although there are no complete experimental data to testify this point, our numerical result is consistent with Tan & Bankoff experimental value [2-13].

Meanwhile, the centroid velocity of a droplet before onset of breakup and the breakup Weber number were investigated by numerical simulations as the droplet is subjected to an impulsive acceleration. As for the centroid velocity, the numerical results agree well with the Pilch & Erdman empirical correlation. The breakup Weber number is little dependent on density ratio, and almost constant and close to 0.4 for the range of density ratio from 1 to 9.

Due to much longer computational time for three-dimensional of the same complexity, we made the dimensional simplification of a sphere droplet into a two-dimensional circular cylinder. Three-dimensional simulations of droplet breakup will be investigated in the next step to unravel quantitatively the effect of dimensional simplification on dynamic behaviors of droplet. After all, we regard the above two-dimensional simulations as a useful exploration for realistic three-dimensional situations and the above conclusions could provide reference for predicting interfacial area in numerically simulating multiphase, multi-fluid and reactive flows involving droplet breakup.

References

2-1) J.O. Hinze, “Fundamentals of the hydrodynamic mechanism of splitting in dispersion processes,” *AIChE Journal*, **1**, 289 (1955).

2-2) J. Han, G. Tryggvason, “Secondary breakup of axisymmetric liquid drops. II. Impulsive acceleration,” *Phys. Fluids*, **13**(6), 1554 (2001).

2-3) M. Pilch, C.A. Erdman, “Use of breakup time data and velocity history data to predict the maximum size of stable fragments for acceleration-induced breakup of a liquid drop,” *Int. J. Multiphase Flow,* **13**, 741 (1987).

2-4) N.I. Kolev, “Fragmentation and coalescence dynamics in multiphase flows,” *Experimental Thermal and Fluid Science,* **6**, 211 (1993).

2-5) B.E. Gelfand, “Droplet breakup phenomena in flows with velocity lag,” *Prog. Energy Combust. Sci.*, **22**, 201 (1996).

2-6) R. S. Brodkey, *The phenomena of fluid motions*, Addison-Wesley, 552 (1967).

2-7) S. Koshizuka, Y. Oka, “Moving-particle semi-implicit method for fragmentation of incompressible fluid,” *Nuclear Science and Engineering,* **123**, 421 (1996).

2-8) H.Y. Yoon, S. Koshizuka, Y. Oka, “Direct calculation of bubble growth, departure, and rise in nuclear pool boiling,” *Int. J. Multiphase Flow*, **27,** 277 (2001).

2-9) H. Ikeda, S. Koshizuka, Y. Oka, “Numerical analysis of jet injection behavior for fuel-coolant interaction using particle method,” *Journal of Nuclear Science and Technology*. **38**(3), 174 (2001).

2-10) K. Nomura, S. Koshizuka, Y. Oka, “Numerical analysis of droplet breakup behavior using particle method,” *Journal of Nuclear Science and Technology*, ; **38**(12), 1057 (2001).

2-11) H. Lamb, *Hydrodynamics*, 6th ed., Cambridge Univ. Press, Cambridge, 471 (1959).

2-12) S. Zaleski, J. Li, and S. Succi, “Two-dimensional Navier-Stokes simulation of deformation and breakup of liquid patches,” *Phys. Rev.Lett*., 75, 244 (1995).

2-13) S. Mortazavi and G.Tryggvason, “A numerical study of the motion of drops in Poiseuille flow. Part 1. Lateral migration of one drop,” *J. Fluid Mech*., 411, 325 (2000).

2-14) M. J. Tan, S.G. Bankoff, “On the fragmentation of drops,” *Trans. ASME, J. Fluid Eng.*, **108**, 109 (1986).

2-15) R. H. Rangel, W. A. Sirignano, “Nonlinear growth of Kelvin-Helmholtz instability: Effect of surface tension and density ratio,” *Phys. Fluids,* **31**, 1845 (1988).

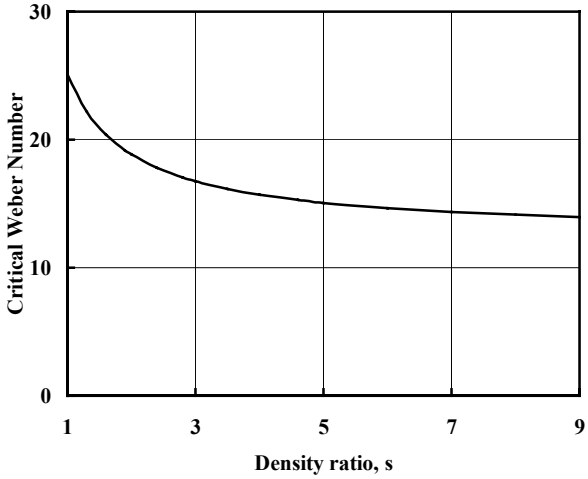

Fig.2-1 We_{cr} vs. density ratio for K-H instability

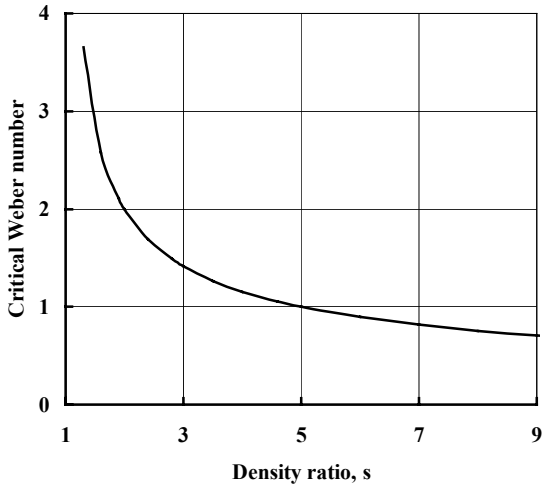

Fig.2-2 We_{cr} vs. density ratio for R-T instability

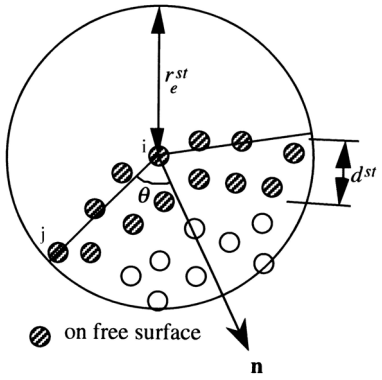

Fig.2-3. Surface tension model

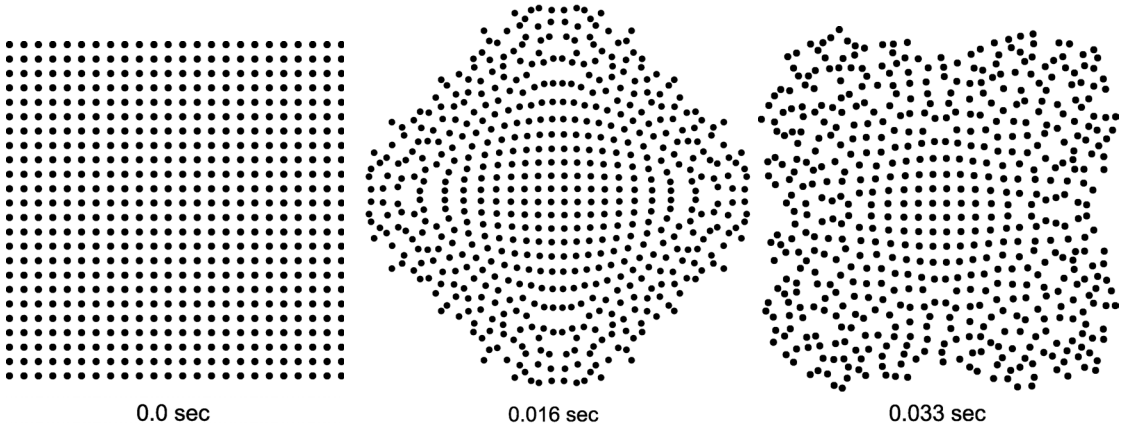

Fig.2-4 Oscillation of an ethanol droplet

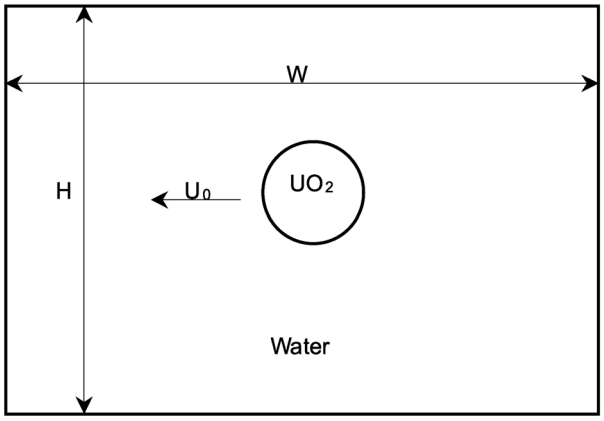

Fig.2-5 Schematic diagram of the computational configuration

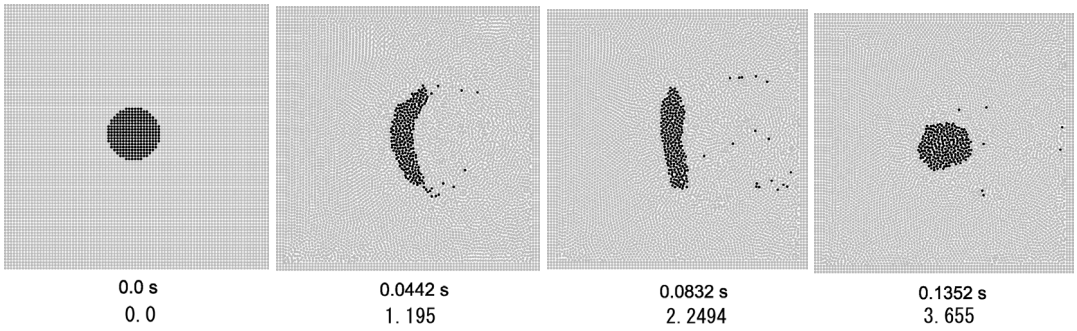

Fig.2-6 Sequence of drop deformation at We=12 and *s*=9

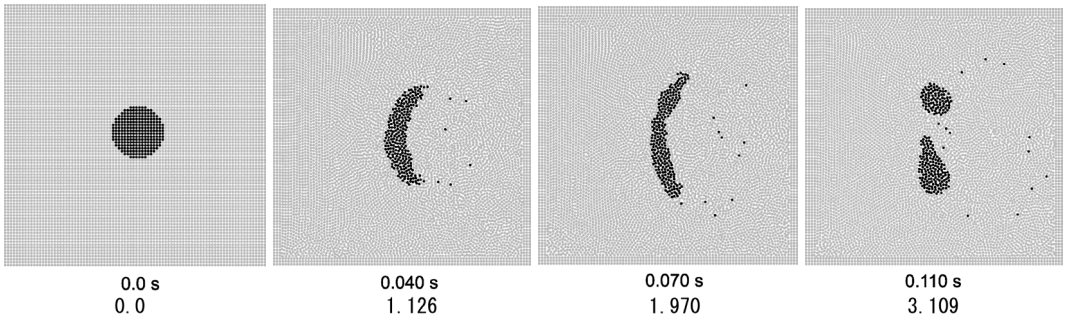

Fig.2-7 Sequence of drop breakup at We=13 and *s*=9

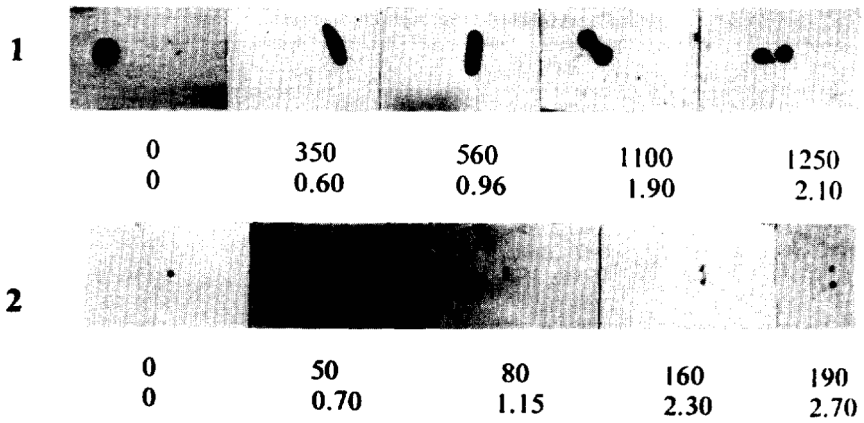

Fig.2-8 Photographic sequences of droplet breakup by vibrational mode by Gelfand [2-5)]

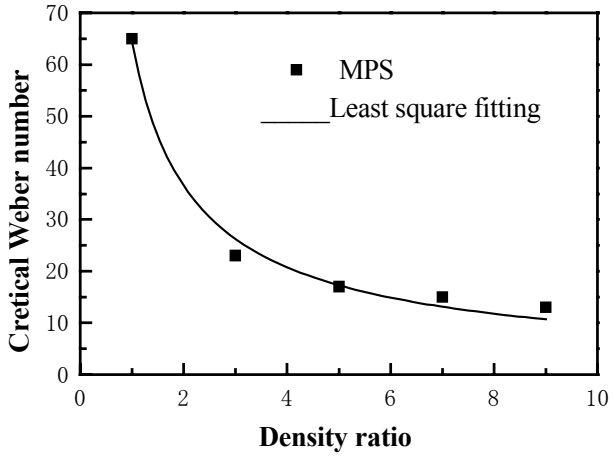

Fig.2-9 Critical Weber number vs. density ratio

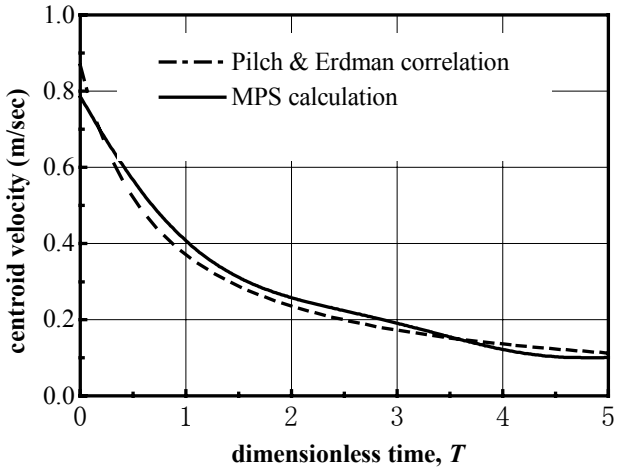

Fig.2-10 Centroid velocity vs. *T* for We=17 and s=5

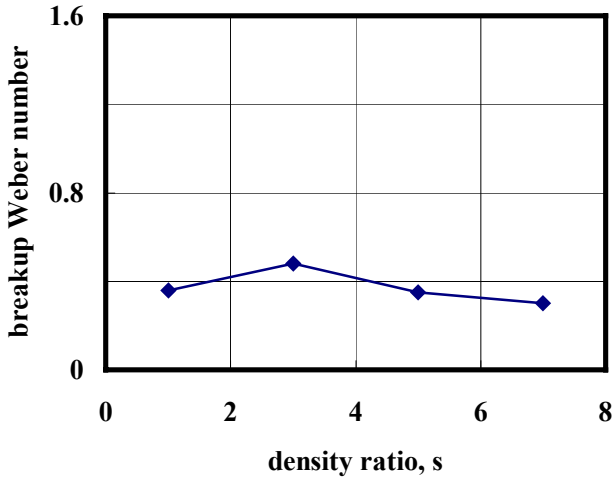

Fig.2-11 Breakup Weber number vs. density ratio

3. Direct Simulation of Flashing Liquid Injection into Liquid

3.1 Introduction

When a pressurized liquid is suddenly discharged into a second ambient liquid with lower pressure than the former corresponding saturation vapor pressure, the liquid becomes superheated (metastable) with respect to the decreased pressure, and a liquid jet may be developed and meanwhile the metastable liquid should be subjected to a fast phase transition process, which is commonly known as flashing liquid injection into liquid. Such a phenomenon is relevant to a multitude of industrial and technological fields intentionally or undesiredly. The former examples can be mentioned as follows: 1) increasing fuel atomization by liquid fuel preheating process for improvement of fuel injector technology, 2) flashing mechanism occurred in expansion device of refrigeration cycle, 3) multi-stage flashing in seawater desalination process. The latter examples can be mentioned as follows: 1) boiling liquid expanding vapor explosion as a consequence of rupture of a pressurized liquefied gas storage tank, 2) rupture of pressurized water pipe in nuclear industry. In this chapter, the motivation to study this phenomenon is involved with one of severe accidents for sodium-cooled fast breeder reactors, that is, the so-called water-leak-into-sodium accident in which some damage or wastage exposes a fully penetrated hole or pore in the wall of heat transfer tubes in steam generators. So water would be leaked into sodium from that hole or pore, where the water pressure is about 17 MPa with temperature in the range of 200~400℃ and however the pressure of liquid sodium is about 0.2 MPa that is much lower than the saturation vapor pressure of the leaked water. Sodium-water reaction (SWR) would

destruct the integrity of the boundary of steam generators and the second circuit loop of sodium-cooled fast breeder reactors. Water flashing in that accident has great effect of SWR. On one hand, two modes of SWR may exist due to the vapor generation of water flashing, viz. liquid water-sodium and vapor-sodium reactions, which have different reaction mechanisms; on another hand, water flashing causes sodium, liquid water and vapor much more mixing and makes the estimation of interfacial area more difficult, which appears as a source term in mass, momentum and chemical reaction rate expressions.

A similar experiment on liquid water injection into atmosphere with flashing was carried out by Edward & O'Brien [3-1)] in a long straight pipe filled with high-temperature, high-pressure water, one end of which was suddenly exposed to atmospheric pressure by bursting a diaphragm. However, their recorded experimental data were limited to the information inside of pipe.

Simoes-Moreira *et al.* [3-2)], using a schlieren setup, carried out iso-octance injection from a small conical convergent nozzle into a low-pressure chamber for the wide range of the depressurization ratio, $R = p_s / p_\infty$, where p_s is the saturation vapor pressure of iso-octance for initial injection temperature. Their taken pictures showed that an emerging jet was formed in a central liquid core even at high R up to1000 and flashing merely occurred on the surface of that liquid core. Meanwhile, it was observed that homogeneous two-phase flow was derived downstream of the jet.

Moreover, Simoes-Moreira *et al.* [3-2)] developed a one-dimensional numerical model to calculate the sudden phase change occurred on the surface of flashing liquid jet. It only yielded limited information due to a lot much simplification. So far, direct

numerical simulations of flashing liquid injection are not yet available in the existing literatures since flashing injection involves the complicated coupling of thermodynamics and hydrodynamics. The objective of the present work is attempted to fill this blank.

Numerical simulation of flashing liquid-liquid injection involves the solution of the Navier-Stokes equations for three fluids coupled with fluid mixing and vapor generation, which offers a special challenge for computational fluid dynamics (CFD) since, on one hand, the actual situations are readily subject to the inception of physical instabilities [3-3)] that can trigger numerically induced instabilities, and on another hand, the surface capture of fluid mixing is yet an obstacle for the existing numerical method of CFD.

As well known, two basic grid-based approaches have been formulated to solve the complex fluid flows with topological change, namely surface tracking and volume tracking, which were reviewed by Hyman [3-4)]. In surface tracking method, interface is characterized by computational elements, such as a string of particles, which are convected with flow. Tryggvason and Unverdi [3-5)] used an additional grid with infinite thickness that is convected with flow. In volume tracking method, markers are used such as in marker and cell (MAC) method [3-6)] or a marker function is convected by flow as in the volume of fluid (VOF) method [3-7)]. Although these methods have been successfully applied to some complex flows with large interfacial deformation, it seems a formidable obstacle for their implementation to mixing of multiple fluids and generation of new components.

In this study, the particle-based method, namely the moving particle semi-implicit method (MPS) [3-8)], is used, which has been successfully applied to many complex flows

with large topological change [3-9~11]. The MPS method is based on fully Lagrangian description. Fluid is modeled as a collection of particles, which move under hydrodynamic forces; numerical diffusion does not arise because the convection terms are not discretized. Grids are not necessary; large deformation of interface can be analyzed without grid tangling. The governing equations of fluid motion (the Navier-Stokes equations) are discretized using moving particles and their interactions. It is very simple and easy to implement. The method can handle fluid mixing seamlessly without special treatment and simulate multiphase flows with minimal modifications.

The purpose of this work is to provide numerical visualization of the flashing liquid-liquid injection by direct numerical simulation and explore the injection behaviors and characteristics. The rest of this study is organized as follows. In Section 2, the surface boiling is identified as the evaporation mode for flashing according to the experimental evidences and theoretical analyses. The physical description and mathematical formulation of flashing liquid injection into liquid are presented in Section 3, and the numerical method and flashing model are also shown in this section. Our results and discussion are demonstrated in Section 4. The conclusion appears in Section 5.

3.2 Identification of evaporation mode for flashing

Evaporation mode determines the formation, distribution, and propagation of liquid-vapor interface in the bulk of superheated liquid, which is an indispensable initial condition to model flashing process. In existing evaporation modes, it is often postulated as homogeneous nucleation in the bulk of liquid and heterogeneous

nucleation on arbitrary wall sites with classical bubble growth.

However, there are clear evidences that a totally different phenomenon, namely surface boiling, can also occur for flashing process especially at sudden depressurization of liquid. Grolmes & Fauske [2-12)] performed the first experiments on suddenly exposing superheated liquid to low-pressure atmosphere with completely suppressed homogeneous and heterogeneous nucleation. They observed that flashing was restricted to the liquid level and the original smooth liquid level underwent instability and quickly broke up with the ejection of a large number of droplets.

In absence of nucleation sites on wall, homogeneous nucleation could be initiated in higher superheat (or higher pressure decay for sudden depressurization). Otherwise, when pressure decay is not high enough to initiate homogenous nucleation in the bulk of liquid and meanwhile no nucleation sites for heterogeneous nucleation are offered on wall, surface boiling should play a dominant role in flashing [3-13)].

However, a series of experiments performed by Simoes-Moreira *et al.* [3-2)] demonstrated that surface boiling could be extended to high pressure decay as a dominant flashing mode for sudden depressurization of liquid. Reinke & Yadigaroglu [3-14)] further concluded from their experiments with 21 of propane, butane, refrigerant R-134a and water that only two different vaporization modes appear in a liquid evaporation under sudden depressurization: slow bubbling below a certain threshold of superheat and surface boiling above this threshold, which is about 5.8k for water at 1 bar backpressure (see their Table 3-1).

The reason for surface boiling to hold at high pressure decay can be explained as follows [3-15)]. Across the liquid-vapor interface we must require conservation of mass and

normal momentum (as shown in Fig.3-1), which are expressed by

$$J = \rho_l (\mathbf{u}_l - \mathbf{v}) \cdot \mathbf{n} = -\rho_g (\mathbf{u}_g - \mathbf{v}) \cdot \mathbf{n} \tag{3-1}$$

$$J(\mathbf{u}_g - \mathbf{u}_l) \cdot \mathbf{n} + p_g - p_l = -\zeta \nabla \cdot \mathbf{n} \tag{3-2}$$

It is observed that the pressure acting on the interfacial liquid side, p_l, exceeds that on the interfacial vapor side, p_g, by an amount specified by the above mass and momentum boundary conditions (3-1) and (3-2) at neglecting the surface tension.

$$p_l = p_g + J^2 \left(\frac{1}{\rho_g} - \frac{1}{\rho_l} \right) \tag{3-3}$$

which shows that liquid phase is not completely relaxed to vapor pressure (here p_g). Such effect is caused by the expansion of the fluid particles undergoing the transition from liquid to vapor so as to seemingly "push back" on liquid [3-3]. Grolmes & Fauske [3-12] also noted in their experiments that the pressure in liquid away from the interface was much greater than that in the low-pressure reservoir to which the liquid was exposed. So homogeneous nucleation should be precluded or ignored in modeling flashing injection even for large pressure decay.

3.3 Problem statement and mathematical formulation

3.3.1 problem definition

The flow configuration investigated here is shown in Fig.3-2. It is assumed that the high-pressure liquid (fluid 1) is suddenly discharged rightward with flashing into a low-pressure tank filled with a second liquid (fluid 2), which is initially quiescent. The vapor generated by flashing of fluid 1 is named fluid 3. The distance from the centerline

(also axis of symmetry) of nozzle to the top or bottom of the tank is L_1, and the distance from the nozzle exit to the outflow boundary of the tank is L_2. The inflow boundary condition of velocity of fluid 1 is with the uniform profile, U_0, from the nozzle exit. The following hypotheses are made in the following simulations:

a) The vapor generated by flashing is assumed as incompressible fluid.

b) The thermodynamic influences are not considered except for evaporation, that is to say, no heat transfer between fluid particles.

c) No chemical reaction exists in the system.

d) Interfacial tension force is just imposed on the jet surface of fluid 1. When it is entrained away from the jet with vapor flow, interfacial tension force is ignored.

e) The gravitational force is ignored.

3.3.2 mathematical formulation and numerical method

The hydrodynamics of liquid injection is governed by a time-dependent momentum equation in the conservative form.

$$\frac{D\rho\,\mathbf{u}}{Dt} = -\nabla p + \nabla\cdot\mu\left(\nabla\mathbf{u} + \nabla\mathbf{u}^T\right) + \zeta\kappa\delta\mathbf{n} \tag{3-4}$$

Equation (3-4) is coupled with a continuity Eq. (3-5):

$$\nabla\cdot\mathbf{u} = 0 \tag{3-5}$$

and the state Eq. (3-6):

$$\frac{D}{Dt}\rho = 0, \text{ and } \frac{D}{Dt}\mu = 0 \tag{3-6}$$

In the present chapter, a two-dimensional Cartesian coordinate is built up. The boundary condition along the tank wall, except the nozzle exit and outflow region in the

right wall, is set as non-slip wall condition.

The above governing equations are solved by the MPS method. Differential operators in the governing equations, such as gradient, divergence and Laplacian operator, are transformed to equivalent particle interactions using a weight function. A semi-implicit algorithm is employed for incompressible flows. The incompressibility constraint is implicitly satisfied by solving a Poisson equation of pressure, while the other terms in momentum equations are explicitly calculated. The detail is shown as follows.

In the MPS method, the differential operators in the governing equations are modeled by particle interactions, which are limited among neighboring particles covered with a weight function:

$$w(r)=\begin{cases}\dfrac{r_0}{r}-1 & 0\le r<r_0\\ 0 & r_0\le r\end{cases} \qquad (3\text{-}7)$$

where r_0 is taken as 2.1 l_0. Summation of the weight functions is called particle number density, n_i, which is used as a normalization factor for averaging.

$$n_i=\sum_{j\neq i} w\left(\left|\mathbf{r}_j-\mathbf{r}_i\right|\right). \qquad (3\text{-}8)$$

The particle number density represents its fluid density. It should be constant for incompressible flows: $n_i=n^0$, where n^0 is dependent on the initial arrangement of particles.

The gradient, divergence and a certain differential operator of the two above combination in the governing equations are transformed to equivalent particle interactions. If Φ and $\mathbf{u}$ are an arbitrary scalar and vector, particle interaction models for

differential operators are expressed as

$$\left\langle \nabla \Phi \right\rangle_i = \frac{d}{n^0} \sum_{j \neq i} \left[\frac{\Phi_j - \Phi_i}{\left| \mathbf{r}_j - \mathbf{r}_i \right|^2} \left(\mathbf{r}_j - \mathbf{r}_i \right) w\left(\left| \mathbf{r}_j - \mathbf{r}_i \right| \right) \right] \tag{3-9}$$

$$\left\langle \nabla \cdot \mathbf{u} \right\rangle_i = \frac{d}{n^0} \sum_{j \neq i} \left[\frac{\left(\mathbf{u}_j - \mathbf{u}_i \right) \cdot \left(\mathbf{r}_j - \mathbf{r}_i \right)}{\left| \mathbf{r}_j - \mathbf{r}_i \right|^2} w\left(\left| \mathbf{r}_j - \mathbf{r}_i \right| \right) \right] \tag{3-10}$$

$$\left\langle \nabla \cdot \beta \nabla \Phi \right\rangle_i = \frac{2d}{n^0} \sum_{j \neq i} \left[\beta_{ij} \left(\Phi_j - \Phi_i \right) \frac{w\left(\left| \mathbf{r}_j - \mathbf{r}_i \right| \right)}{\left| \mathbf{r}_j - \mathbf{r}_i \right|^2} \right] \tag{3-11}$$

where β_{ij} is defined as

$$\beta_{ij} = \frac{\beta_i + \beta_j}{2} \tag{3-12}$$

The gradient model, Eq. (3-9), is obtained as the average of gradient vectors that are determined between the *i*th particle and its neighborings. The combination operator, Eq. (3-11), is derived from the physical concept of diffusion. Substituting the above particle interaction models into the governing equations, we can obtain the particle dynamics to simulate fluid flows. More detail is described in the reference [3-8)].

The Navier-stokes equations are solved by the semi-implicit algorithm. For every time step, the surface tension force and viscous force in the momentum conservation equation are computed explicitly. Temporary particle locations **r*** and velocities **u*** are computed from the positions $\mathbf{r}^n$ and velocities $\mathbf{u}^n$ of the previous time step as follows:

$$\mathbf{u}^* = \mathbf{u}^n + \frac{dt}{2\rho} \left[\nabla \cdot \mu \left(\nabla \mathbf{u} + \nabla \mathbf{u}^T \right) \right] \tag{3-13}$$

and

$$\mathbf{r}^* = \mathbf{r}^n + \mathbf{u}^* dt \tag{3-14}$$

However, the incompressibility constraint may not be satisfied, that is to say, the temporal particle number density n^* is not n^0. So the temporal value n^* should be implicitly corrected to n^0 by

$$n' = n^0 - n^* \tag{3-15}$$

where n' is related to the velocity correction $\mathbf{u}'$ through the mass conservation equation:

$$\frac{1}{\Delta t}\frac{n'}{n^0} = -\nabla \cdot \mathbf{u}' \tag{3-16}$$

The velocity correction is derived from the implicit pressure gradient term as

$$\mathbf{u}' = -\frac{\Delta t}{\rho}\nabla p^{n+1} \tag{3-17}$$

With Eqs.(3-15)~(3-17), a Poisson equation of pressure is obtained:

$$\nabla \cdot \frac{1}{\rho}\nabla p_i^{n+1} = -\frac{1}{\Delta t^2}\frac{n^*_i - n^0}{n^0} \tag{3-18}$$

The solving of the pressure equation is further divided into two stages with respect to heavy particles (liquid phase) and light particles (vapor phase) to stabilize the calculation, because large density ratio of liquid and vapor phase leads to a large condition number of the coefficient matrix of pressure equation. In the first stage, light particles are ignored, where the Dirichlet boundary condition is imposed on an interfacial heavy particle. In the second stage, heavy particles are treated as wall condition, where homogeneous Neumann condition is imposed on interfacial heavy and light particles. More details can be referred to Koshizuka et al. [3-16]. The above Poisson equation of pressure is solved by the Incomplete Cholesky Preconditioning Conjugate

Gradient (ICCG) linear solver. Then the velocities and the positions of particles are modified by pressure gradient.

3.3.3 flashing model

The non-equilibrium vapor generation is one of the most important features of liquid flashing as pressure suddenly decays. It manifests itself by the liquid failure to begin evaporation when saturation condition is reached, leading to metastable condition of liquid. As a consequence, flashing starts with some delay and thus the real vapor quality pattern may essentially differ from the equilibrium one.

Jones & Saha [3-17)] made a comprehensive review on the existing flashing models. Relaxation models suggested by Bauer *et al.* and Jones (references seen in Jones & Saha paper), as they pointed out, seem to show promise in describing the effects of thermal non-equilibrium from phenomenological viewpoint. It is of nature to adopt it to model flashing process. Here, we will briefly describe one of them, Homogeneous Non-equilibrium Relaxation Model (HRM), suggested by Downar-Zapolski *et al.* [3-18)].

The vapor generation rate, Γ, plays a fundamental role in liquid flashing. This function, which reflects the whole complicated process of flashing, may depend not only on the flow parameters but also on the number and structure of pre-existing interfaces (liquid-gas or liquid-solid) in metastable liquid. Being conscious of the complexity of the problems and knowing that the vapor mass production rate vanishes when the vapor quality, x, reaches its unconstrained equilibrium value, x_e, the HRM model uses linear approximation to treat the above complexity by extracting the first term from a Taylor series expansion of the vapor generation rate, Γ, which takes the

form

$$\frac{Dx}{Dt} = \frac{\Gamma}{\rho_m} = \frac{x_e - x}{\tau} \tag{3-19}$$

so

$$\Gamma = \rho_m \frac{x_e - x}{\tau} \tag{3-20}$$

It can be seen that Eq. (3-20) builds an exponential tendency toward an unconstrained equilibrium from an initial quality x_0. The parameters of Eq. (3-20) are calculated as shown in the following:

a) ρ_m is the mixture density.

$$\frac{1}{\rho_m} = \frac{x}{\rho_g} + \frac{1-x}{\rho_l} \tag{3-21}$$

so

$$\rho_m = \frac{\rho_g \rho_l}{x\rho_l + (1-x)\rho_g} \tag{3-22}$$

b) x_e is the equilibrium vapor quality. There are two choices for x_e, namely isentropic quality, x_s, and isenthalpic quality, x_h, which are defined respectively as

$$x_s = \frac{s - s_{sl}(P_\infty)}{s_{sg}(P_\infty) - s_{sl}(P_\infty)} \quad < \quad x_h = \frac{h - h_{sl}(P_\infty)}{h_{sg}(P_\infty) - h_{sl}(P_\infty)} \tag{3-23}$$

As well known, the definition of the isenthalpic quality assumes that the vapor/liquid mixture is at rest after vaporization; this results in the highest possible quality since no latent heat is converted to kinetic energy. In contrast, the isentropic quality results in maximum conversion to kinetic energy, thus leading to the lowest quality. Reinke and Yadigaroglu [3-14)] experiments showed that the derived quality values

from measured boiling front velocity are between these two limiting cases and very near the isenthalpic line case (see its Fig.3-10). So the phase-change at the boiling front should be described as isenthalpic, not an isentropic as often proposed, taken as $x_e = x_h$. Thus, the initial velocity of the vapor particles generating by flashing should be set to zero.

c) Vapor quality, *x,* is calculated based on its equivalent dependence on void fraction

$$\alpha = \frac{x\rho_m}{\rho_g} \Rightarrow x = \alpha \frac{\rho_g}{\rho_m} \tag{3-24}$$

where α for each flashing particle is locally calculated as shown:

$$\alpha = \frac{mV_g}{mV_g + V_l} \tag{3-25}$$

d) τ is the relaxation time, which is a function of void fraction and pressure decay amount. Downar-Zapolski *et al.* [3-18)] used a power function to fit the dependence of τ on void fraction and pressure decay amount from Reocreux's Moby Dick experimental data (references seen in its paper) as follows.

$$\tau = \tau_0 \alpha^{-0.54} \varphi^{-1.76} \tag{3-26}$$

where τ_0=7.57546×10^{-3}s, φ is the non-dimensional pressure decay amount defined as,

$$\varphi = \left[\frac{p_s(T_0) - p_\infty}{p_{cr} - p(T_0)} \right] \tag{3-27}$$

Because surface boiling has been identified as evaporation mode for flashing liquid injection as shown in Sec. 2, it is prescribed that only surface particles of certain liquid patch are subjected to flashing, and internal liquid particles are free from flashing until

they are exposed to surface.

The strategy in incorporating the HRM flashing model with the MPS method is presented as follows. Firstly, liquid particles located on the jet surface are identified using the similar manner as Koshizaka & Oka [3-8] did in free surface flows and marked as interfacial particles, the condition of which triggers the inception of flashing. Then we calculated the vapor generation rate of the interfacial liquid particles as shown in Eq. (3-20). Each flashing liquid particle is associated with a property of the accumulated generated vapor mass. When this value is over the mass of one vapor particle, a new vapor particle is released from it and located near to interface, and meanwhile the mass is subtracted from the accumulated mass. The condition for the flashing termination of a liquid particle is satisfied as its local vapor quality, x, reaches the unconstrained equilibrium vapor quality, x_e.

3.4 Results and discussion

Seven independent dimensionless groups are produced by conducting the dimensional analysis of Eqs. (3-4), (3-5) and (3-20). Those are $\mathrm{Re} = D\rho_1 U_0/\mu_1$, the injected liquid Reynolds number, $\mathrm{We} = DU_0^2\rho_1/\zeta$, the Weber number, ρ_1/ρ_2 and μ_1/μ_2, respectively the density and viscosity ratios of injected fluid 1 and tank fluid 2, ρ_1/ρ_3 and μ_1/μ_3, respectively the density and viscosity ratios of injected fluid 1 and vapor fluid 3, and $R = p_s/p_\infty$, the depressurization ratio. The Re number represents the ratio of inertial to viscous force, the We number represents the ratio of hydrodynamic force to surface tension force, and R represents the pressure decay

amount or superheat. Alternatively, one or more of these dimensionless groups can be replaced by other dimensionless group or their combinations, such as $\varphi = \frac{p_s(T_0) - p_\infty}{p_{cr} - p(T_0)}$ for R and the capillary number, $\mathrm{Ca} = \mathrm{We}/\mathrm{Re}$, for the We number.

Considering our motivation of the present research, the scenario of flashing injection is assumed as the hypothetic water-leak-into-sodium accident in steam generators of fast breeder reactors, in which water subjected to depressurization is suddenly discharged into sodium. The properties of water and vapor and sodium are taken at the normal operation condition of steam generators of fast breeder reactor (shown in Table 3-1). So all the above dimensionless groups but R or φ are fixed at a given nozzle size and the injection velocity of water. The injection velocity of water at such condition can be approximately taken as a constant, which will be discussed below. Our concern in the present research stresses the effect of φ or R on flashing injection behavior, which is a function of the location of water leak site in steam generators.

Herein, we wish to comment briefly on the injection velocity of flashing liquid, which is somewhat different from purely hydrodynamic liquid-liquid jet. It is well known that the speed of sound in liquid is far greater than that in vapor or gas and thus liquid cannot become easily choked except at extremely high injection pressure. However, Simoes-Moreira *et al.* [3-2)] experimental data and their mentioned other experimental data on mass flux measurement showed that the mass flux, as a function of the backpressure to injection pressure ratio, becomes independent of the ratio below a certain threshold. As they indicated, it is a puzzling phenomenon, which is not explored in this paper. So it is in the present research assumed that the injection velocity is equal

to the sound speed of the equilibrium two-phase flow corresponding to the metastable liquid, which is determined by the critical flow flux. As mentioned above, we use the isenthalpic homogeneous equilibrium model [3-19] to predict the critical flow flux, as shown in Eq. (3-28).

$$J_{cr} = \left\{ \frac{-1}{\dfrac{dv_l}{dp} - \left(\dfrac{v_{\mathrm{lg}}}{h_{\mathrm{lg}}}\right)\dfrac{dh_l}{dp} + x\left[\dfrac{dv_{\mathrm{lg}}}{dp} - \left(\dfrac{v_{\mathrm{lg}}}{h_{\mathrm{lg}}}\right)\dfrac{dh_{\mathrm{lg}}}{dp}\right]} \right\}^{1/2} \tag{3-28}$$

Figure 3-3, calculated by Eq. (3-28), shows the critical flow flux and the assumed water leak rate from a nozzle with 4mm diameter under water temperature 352℃ and the prescribed pressures in Table 3-1. The water leak rate at the critical condition is about 0.13kg/s in vapor quality x=0.0, and the corresponding velocity of water is 8.39m/s, which will be used as the injection velocity in the following simulations.

A uniform particle size is used for water, vapor and sodium in simulations of the MPS method, which is taken as l_0=0.5mm. The effect of the computational dimensions L_1 and L_2 were investigated by sensitivity studies. It was found that the use of L_1/D=12 and L_2/D=4 were large enough to establish insensitivity of injection behaviors.

Numerical simulations at different initial injection temperatures of water were carried out, whose parameters are illustrated in Table 3-2. The simulation results at different cases are shown in Fig.3-4 for the fully shape-relaxed jets, where the black particles (shown in circle) represent the injected water, the light gray particles are the engendered vapor particles due to flashing, and the continuous phase particles in tank is not shown for visual clarity.

Examination of the simulation results allows one to conclude that the consistence with Simoes-Moreira *et al.* [3-2)] experiments of flashing injection is well obtained: a jet emerging from the nozzle remains in the liquid phase and is torn away into a liquid core by surface boiling; and the jet extinguishes downstream of the nozzle exit. The extinction lengths of flashing water jet are shown in Fig.3-5 for different initial injection temperatures marked by solid squares. For comparison, the extinction lengths of iso-octane flashing jet carried out by Simoes-Moreira *et al.* [3-2)] are also presented in Fig. 5 for two different injection pressures respectively marked by solid triangles and circles. It is clearly shown that for a given injection pressure, the extinction length decreases with increasing the initial injection temperature, which is ascribed to the higher evaporation rate at higher initial injection temperature. Although the vapor generation rate is assumed as local linear function of vapor quality, it is in reality a power function on vapor quality due to that the relaxation time is a power function of void fraction. Thus the extinction length of jet is weakly dependent on the initial injection temperature as it is tending to the saturation temperature for the injection pressure.

In addition, the simulation results show that approximate homogeneous two-phase flow is derived downstream of the tip of flashing jet, in which liquid particles are post-flashing water particles that is entrained by vapor flow. It is evident that the vapor quality increases with increasing the initial injection temperature as shown in Fig.3-4.

3.5 Conclusions

Numerical simulations of flashing liquid injection into liquid were carried out by the MPS method incorporated with the homogeneous non-equilibrium relaxation model.

Our numerical simulation results are consistent with Simoes-Moreira *et al.* [3-2)] observations of iso-octane flashing jets: a flashing jet issuing from a nozzle is formed as a central liquid core; the extinction length decreases with increasing injection temperature and tends asymptotically to a constant as the initial injection temperature approaches the saturation temperature corresponding to the injection pressure. The homogeneous two-phase flow is derived which vapor quality increases with increasing the injection initial temperature.

References

3-1) A. R. Edwards, T. P. O'Brien, Studies of phenomena connected with the depressurization of water reactors, *J. Br. Nucl. Energy Soc*. 9 (1970) 125-135.

3-2) J. R. Simoes-Moreira, M. M. Vieira, E. Angelo, Highly expanded flashing liquid jets, *Journal of Thermophysics and Heat Transfer* 16 (3) (2002) 415-424.

3-3) A. Prospertti, M. S. Plesset, The stability of an evaporating liquid surface, *Phys. Fluids* 27 (1984) 1590-1602.

3-4) J. M. Hyman, Numerical methods for tracking interfaces, *Physica D* 12 (1984) 396-407.

3-5) G. Traggvason, S. O. Unverdi, Computations of three-dimensional Rayleigh-Taylor instability, *Phys. Fluids* A 2 (1990) 656-659.

3-6) F. M. Harlow, J. E. Welch, Numerical study of large-amplitude free-surface motions, *Phys. Fluids* 9 (1966) 842-851.

3-7) C. W. Hirt, B. D. Nichols, Volume of fluid (VOF) method for the dynamics of free boundaries, *J. Comput. Phys*. 39 (1981) 201-225.

3-8) S. Koshizuka, Y. Oka, Moving-particle semi-implicit method for fragmentation of incompressible fluid, *Nuclear Science and Engineering* 123 (1996) 421-434.

3-9) H. Ikeda, S. Koshizuka, Y. Oka, Numerical analysis of jet injection behavior for fuel-coolant interaction using particle method, *Journal of Nuclear Science and Technology* 38 (2001) 174-182.

3-10) H. Y. Yoon, S. Koshizuka, Y. Oka, Direct calculation of bubble growth, departure, and rise in nucleate pool boiling, *Int. J. Multiphase Flow* 27 (2001) 277-298.

3-11) R-Q. Duan, S. Koshizuka, Y. Oka, Two-dimensional numerical simulation of

drop deformation and breakup at around the critical Weber number, *Nuclear Engineering and Design* 225 (2003) 37-48.

3-12) M. A. Grolmes, H. K. Fauske, Axial propagation of free surface boiling into superheated liquids in vertical tubes, *Fifth Int. Heat Transfer Conf.*, Tokyo, 1974, pp.30-34.

3-13) E. Hahne, G. Barthau, Evaporation waves in flashing processes, *Int. J. of Multiphase Flow* 26 (2000) 531-547.

P. Reinke, G. Yadigaroglu, Explosive vaporization of superheated liquids by boiling fronts, *Int. J. of Multiphase Flow* 27 (2001) 1487-1516.

3-14) L. D. Landau, E. M. Lifshitz, Fluid Mechanics, Pergamon, New York, 1959, 230-244.

3-15) S. Koshizuka, H. Ikeda, Y. Oka, Numerical analysis of fragmentation mechanisms in vapor explosions, *Nuclear Engineering and Design* 189 (1999) 423-433.

3-16) O.C. Jones, P. Saha, Non-equilibrium aspects of water reactor safety, *Symposium on the thermal and hydraulic aspects of nuclear reactor safety*, Brookhaven, Vol.1 (1977) 249-288.

3-17) P. Downar-Zapolski, Z. Bilicki, L. Bolle, J. Franco, The non-equilibrium relaxation model for one-dimensional flashing liquid flow, *Int. J. Multiphase Flow*. 22 (1996) 473-483.

3-18) E. Elias, G. S. Lellouche, Two phase critical flow, *Int. J. of Multiphase Flow* 20 (suppl.) (1994) 91-168.

Table 1 Normal operation conditions for steam generators of fast breeder reactor

[**Water and vapor**]		
• Temperature	200~352	℃
• Pressure	17.0	MPa
[**sodium**]		
• Pressure	0.2	MPa

Table 2 Numerical simulation cases studied

Run	T_0 /℃	$p_s(T_0)$ /MPa	φ	R	x_e
1	200	1.56	0.2685	7.8	0.1588
2	220	2.33	0.4206	11.65	0.2000
3	240	3.36	0.6232	16.78	0.2413
4	260	4.69	0.8866	23.45	0.2843
5	280	6.43	1.2301	32.15	0.3292
6	300	8.61	1.6607	43.05	0.3740
7	320	11.31	2.1939	56.55	0.4308
8	340	14.62	2.8475	73.10	0.4876
9	352	17.00	3.3175	85.00	0.5160

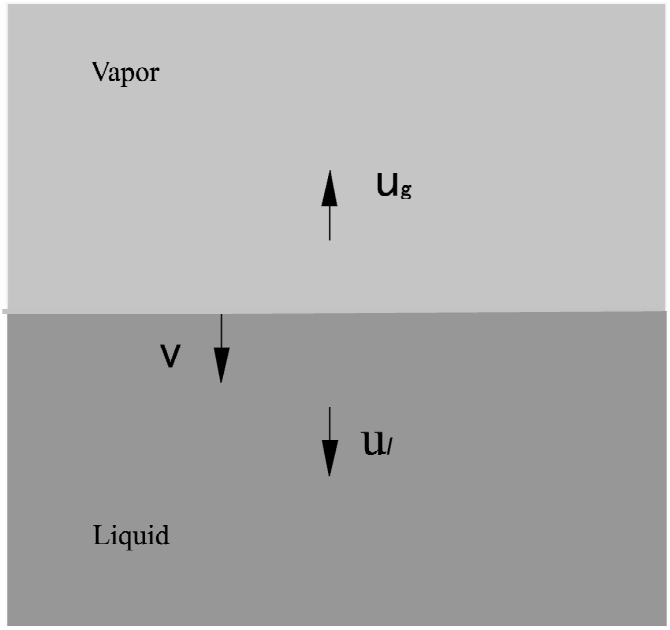

Fig.3-1 Boundary condition of liquid-vapor interface at liquid flashing

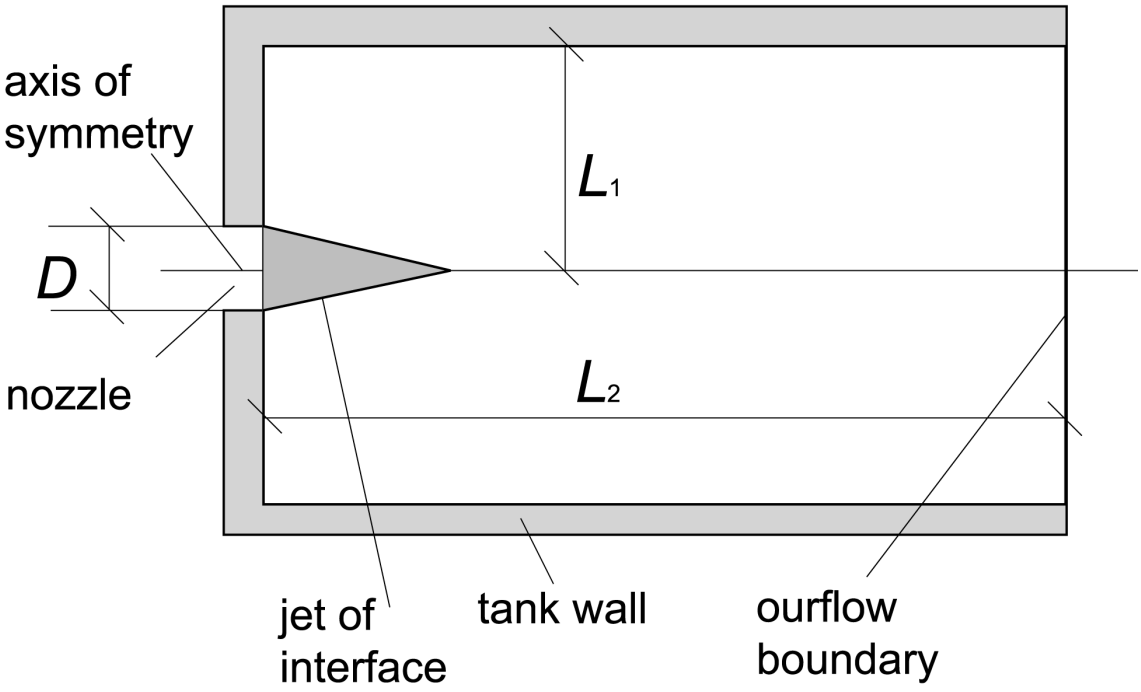

Fig.3-2 Schematic configuration of flashing liquid jet into liquid

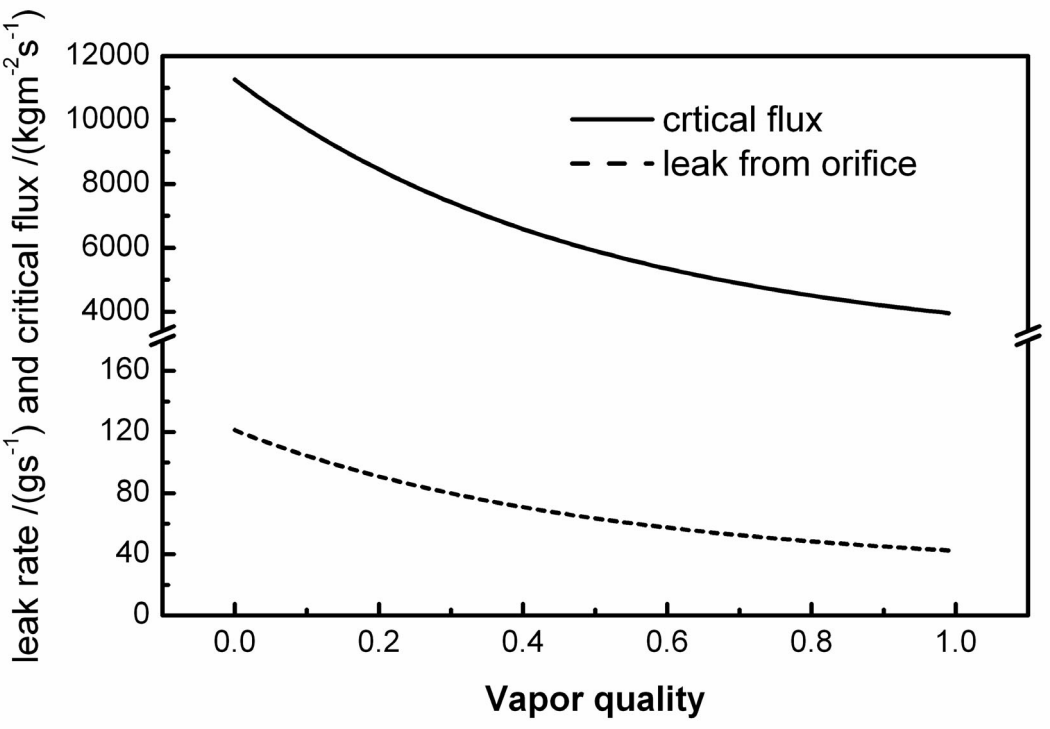

Fig.3-3 Critical flow flux and water leak rate at D=4mm, T=352°C, p=17MPa and p_{∞}=0.2MPa, predicted by the isenthalpic homogeneous equilibrium model

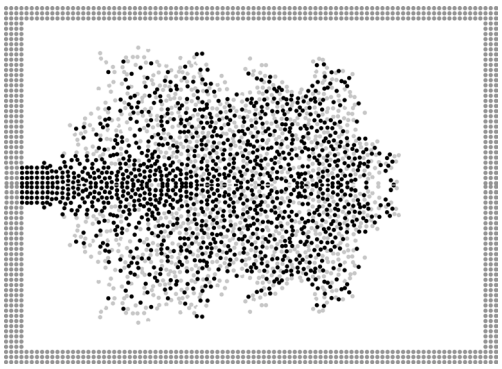

(1) T=200℃

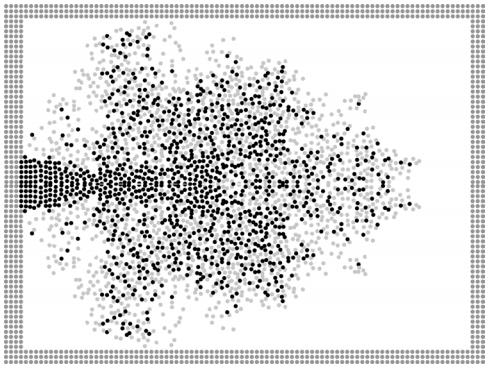

(2) T=220℃

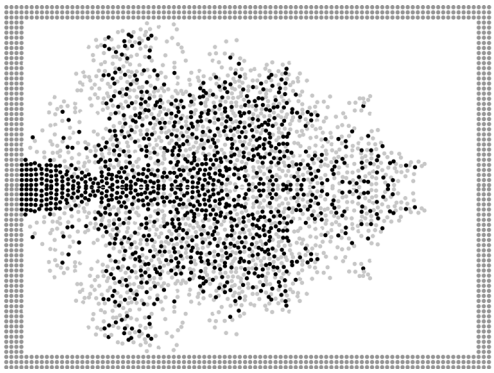

(3) T=240℃

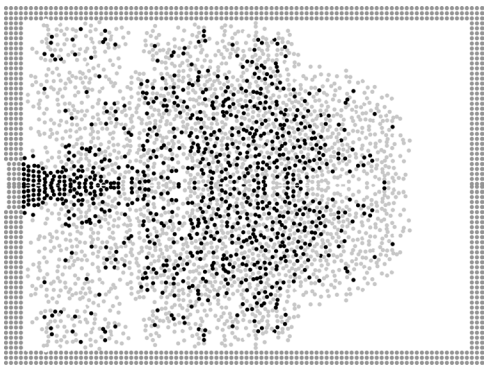

(4) T=260℃

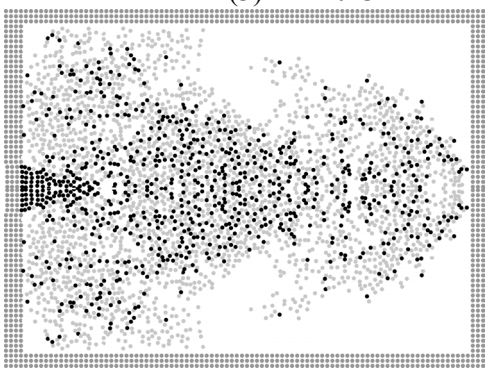

(5) T=280℃

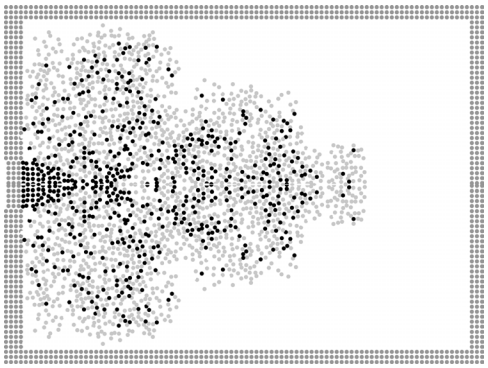

(6) T=300℃

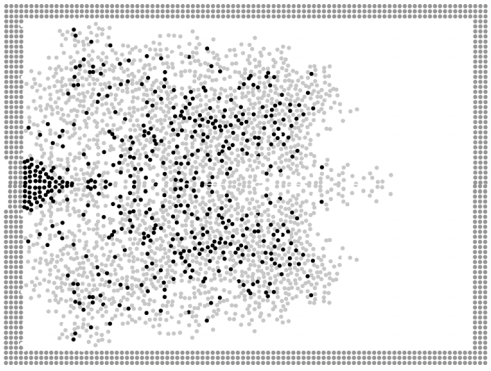

(7) T=320℃

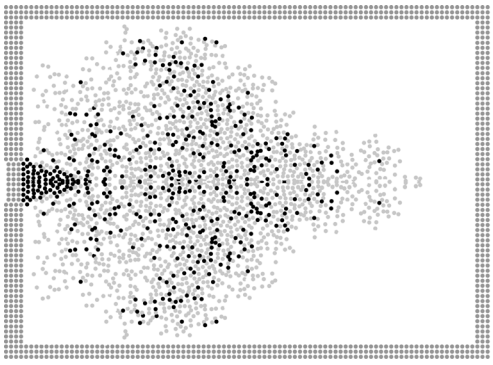

(8) T=340℃

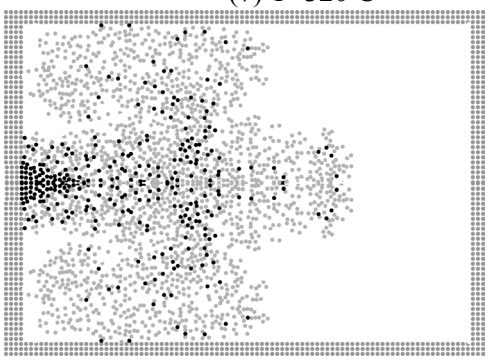

(9) T=352℃

Fig.3-4 Series of flashing water injection into sodium by direct simulation for different initial injection temperatures

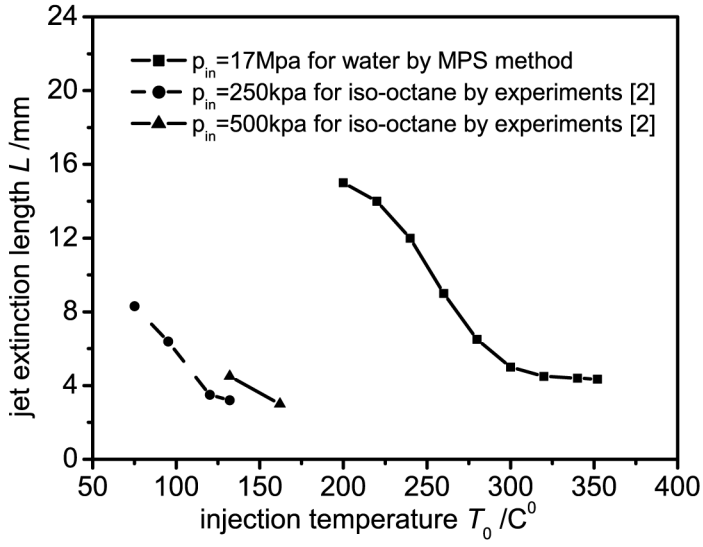

Fig.3-5 Extinction length of flashing jet as function of the initial injection temperature

4. Estimation of Interfacial Area for Flashing Water Injection into Sodium

4.1 Introduction

Water leakage into sodium in steam generators is one of severe hypothetical accidents for Liquid Mental Fast Breeder Reactors (LMFBR). Sodium Water Reaction (SWR) is highly exothermic, instantaneous and irreversible, creating high temperature to vaporize part of reaction products and causing undesirable pressure surges and wastage of adjacent tubes. The accident is a complex phenomenon, involved with thermal hydrodynamics and chemical reaction. As commonly known, the overall SWR reaction rate is limited by physical rather than chemical kinetics in that this reaction is instantaneous; specifically the chemical reaction rate is determined by interfacial area between sodium and water (liquid or vapor). Thus sufficient information of interfacial area is needed for prediction of severity of this accident.

On the other hand, with regard to numerical computation of multi-phase flows concerning with SWR, the significance of estimating interfacial area is concerned with the application of two-fluid flow model, which is the most widespread model to simulate multi-fluid flows. Interfacial area between different fluids appears in interfacial transport correlations and chemical reaction rate. Thus the determination of interfacial area is of the utmost importance to exactly predict the evolution of the complex SWR flows.

At occurrence of fracture of heat transfer tubes in steam generators, pressurized

water (17MPa) inside of tubes is suddenly discharged with flashing into lower-pressure sodium (0.2MPa) than the corresponding saturation pressure of water. As known from Duan et al. [4-1)] direct simulation results of flashing injection (seen in Fig.4-1) and Simoes-Moreira et al. [4-2)] experimental observations of highly expanded flashing liquid jets (seen in Fig.4-2), a cone-shape jet would be developed in that flashing is just restricted on the surface of jet; meanwhile homogeneous two-phase flow would be derived downstream of jet. For the estimation of interfacial area between sodium and water, it is usually thought that creation of interfacial area is engendered by two successive disintegrations: the primary one is the flashing jet breakup into drops, and the secondary one is the drop breakup until its length scale satisfies a certain stability criterion [4-3)]. So we will consider the two breakup processes in our strategies of estimating interfacial area of SWR. In the present chapter, it is assumed that the above two breakup processes are mainly dominated by thermal hydrodynamic effect without account of chemical reaction.

The rest of the chapter is organized as follows. The strategy to estimate interfacial area is described in Section 2. In Section 3, we present the main results and discussion. Our conclusions appear in Section 4.

4.2 Strategy to estimate interfacial area

Roughly speaking, the strategy of estimating interfacial area for flashing water injection into sodium can be described as follows. Based on the numerical visualization of flashing jets from Duan et al. [4-1)], the technique of box-counted statistics [4-4)] is used to partition the flow field into small λ-size boxes. Herein, it is assumed that liquid

component of interest ultimately accumulates in drops as dispersed phase and the other components constitute homogeneous mixture as continuous phase. The hydrodynamic stability criterion is imposed on drop to estimate its length scale and number of drops in each box. More details will be given in the following.

Firstly, the stability criterion of drop in another immiscible fluid will be discussed. Dimensional analyses show that the critical Weber number ($\mathrm{We}_{\mathrm{cr}} = \rho_c d_0 u_0^2 / \sigma$) of drop breakup under impulsive acceleration is dependent on the Reynolds number, $\mathrm{Re} = u_0 d_0 \rho_c / \mu_c$, the Ohnesorge number, $\mathrm{On} = \mu_d / (\rho_d d_0 \sigma)^{1/2}$, and the density ratio, ρ_d / ρ_c , where d_0 and u_0 denote the initial drop diameter and the relative velocity between drop and surrounding fluid respectively, ρ_c is the density of surrounding fluid, ρ_d is the density of drop, μ_d is the viscosity of drop, and σ is the interfacial tension coefficient. Experiments [4-5), 4-6)] showed that the Re number has little effect on the critical Weber number. Thus the dependence of the critical Weber number can be expressed as:

$$\mathrm{We}_{\mathrm{cr}} = f(\mathrm{On}, \rho_d / \rho_c) \tag{4-1}$$

Furthermore, Brodkey [4-7)] pointed out that the critical Weber number is little dependent on the Ohnesorge number when it is small (On<0.1), which is satisfied for almost all Newtonian fluids. So Eq. (4-1) would be simplified for On<0.1 as:

$$\mathrm{We}_{\mathrm{cr}} = f(\rho_d / \rho_c) \tag{4-2}$$

We have used the MPS method to directly simulate the drop breakup in another immiscible fluid under impulsive acceleration [4-8)] as shown in Fig.4-3. And moreover the dependence of $\mathrm{We}_{\mathrm{cr}}$ on density ratio was explored in the reference [4-9)], which is fitted

by the least square method on power function as follows:

$$\mathrm{We}_{\mathrm{cr}} = 64.36\left(\rho_d / \rho_c\right)^{-0.82} \tag{4-3}$$

Direct simulation results of flashing injection [4-1)] have demonstrated that interfacial evolution of flashing injection exhibits convoluted and complex dynamics and structures. As mentioned above, it is assumed that liquid water and sodium would exist in the form of spheroid, whose length scale should meet the stability criterion of Eq. (4-3). Quantitative examinations of mixed-fluid interface have mostly relied on box-counted statistics [4-4)]. A large-scale flow domain of interest containing interface is partitioned into smaller uniform λ-size boxes (as shown Fig.4-4), whose size should be larger than the possible maximum stable scale of drop over all λ-size boxes. The component volume fraction, $\alpha^{\lambda}_{(\mathrm{i})}$, of each box is calculated based on the ratio of the particle number of a certain component, $n^{\lambda}_{(\mathrm{i})}$, to the total particle number of all components in that box, as shown in Eq. (4-4).

$$\alpha^{\lambda}_{(i)} = \frac{n^{\lambda}_{(i)}}{\sum_{j=1}^{m} n^{\lambda}_{(j)}} \tag{4-4}$$

where it is assumed that all particles have the same volume for all components, m is the number of components in the system, superscript λ represents the qualities pertaining to λ-size box, subscripts with bracket denote the qualities of component i, and in the following subscripts without bracket denote the qualities of the MPS particles.

The component velocity for each box, $\mathbf{u}^{\lambda}_{(\mathrm{i}),}$ is taken as the average of velocity vector superposition for all particles of that component in box.

$$\mathbf{u}_{(i)}^{\lambda} = \frac{\sum_{j}^{n_{(i)}^{\lambda}} \mathbf{u}_{j}^{\lambda}}{n_{(i)}^{\lambda}} \tag{4-5}$$

where $\mathbf{u}_{j}^{\lambda}$ is the velocity of particle *j*.

The next important step is the estimation of the length scale of drops in each box. It is possible to proceed in different ways, but one seems to be easy and practicable. It is assumed that dispersed phase (herein sodium or liquid water) is locally monodisperse, that is, the length scale of all drops in each λ-size box is same but may be different from each other. As mentioned above, the length scale of drop is calculated based on the critical Weber number, of which the characteristic velocity is taken as the relative velocity between drop and its surrounding fluid mixture; and the density ratio in Eq. (4-3) is taken as the ratio of drop to its surrounding fluid mixture. The velocity and density of surrounding fluid mixture in each λ-size box are calculated as follows (taking drop as component *i*):

$$\mathbf{u}_{(i,mix)}^{\lambda} = \frac{\sum_{j=1, j\neq i}^{m} \mathbf{u}_{(j)}^{\lambda} \alpha_{(j)}^{\lambda}}{\sum_{j=1, j\neq i}^{m} \alpha_{(j)}^{\lambda}} \tag{4-6}$$

$$\rho_{(i,mix)}^{\lambda} = \frac{\sum_{j=1, j\neq i}^{m} \rho_{(j)}^{\lambda} \alpha_{(j)}^{\lambda}}{\sum_{j=1, j\neq i}^{m} \alpha_{(j)}^{\lambda}} \tag{4-7}$$

In this case, the division of product of λ-size box volume, V^{λ}, and the component volume fraction, $\alpha_{(i)}^{\lambda}$, by the volume of one single drop, $\pi d_0^3/6$, gives the number of drops in box:

$$\beta_{(i)}^{\lambda} = \frac{V^{\lambda}\alpha_{(i)}^{\lambda}}{\pi d_0^3/6} \tag{4-8}$$

So for the locally monodisperse system, there is a unique relationship between component volume fraction, local length scale of drop, and interfacial area density (it is defined as interfacial area $F_{(i)}{}^{\lambda}$ divided by λ-size box volume V^{λ}).

$$\frac{F_{(i)}^{\lambda}}{V^{\lambda}} = \frac{\beta_{(i)}^{\lambda}F_d}{V^{\lambda}} = \frac{\alpha_{(i)}^{\lambda}}{\pi d_0^3/6}4\pi d_0^2 = \frac{24\alpha_{(i)}^{\lambda}}{d_0} \tag{4-9}$$

where F_d is the surface area of one drop.

Another parameter of interfacial area properties is the total interfacial area generated by flashing injection, which could be used to roughly estimate the overall SWR rate in the water-leak-into-sodium accident. It can be obtained by summing up interfacial area in each λ-size box over the computational domain.

The above strategy for estimation of interfacial area is schematically reflected in Fig.4-5.

4.3 Results and discussion

4.3.1 volume fractions and velocities

Four types of λ-size box partition were made on the direct simulation results of flashing water injection into sodium, viz. λ=2, 4, 6, 8δ, herein δ, taken as 5e-4m, is the particle scale used in the MPS method. The series in Figs.4-6 show respectively the contour of volume fractions and velocities of vapor, liquid water and sodium at the initial injection temperature T=220°C for λ=2δ partition. The cases at other initial injection temperatures and other λ-size box partitions have also been investigated but

are not presented for the sake of conciseness. Nevertheless, their general behaviors are similar to that of the selected series.

4.3.2 total interfacial area for sodium and liquid water

Two interfacial areas were investigated, viz., the interfacial area between liquid water and its surrounding fluid mixture (sodium and vapor) and the interfacial area between sodium and its surrounding fluid mixture (liquid water and vapor). Herein, it should be recalled that the two interfacial areas are estimated based on three dimensions, wherein the third dimension, z, is assumed 1 meter, although our simulations were carried out two-dimensionally.

Two different critical Weber numbers were chosen to estimate interfacial area. The first was taken as constant, $We_{cr} = 64.36$. The series in Fig.4-7 show the interfacial area between sodium and its surrounding mixture at different initial injection temperatures respectively for λ-size box partitions λ=2, 4, 6, 8δ. Another interfacial area between liquid water and its surrounding mixture at different initial injection are shown in the series in Fig.4-8 for the above four λ-size box partitions.

The second choice of the critical Weber number was taken as Eq. (4-3). The above two interfacial areas are presented respectively in the series in Figs.4-9 and 4-10. It is shown from the above figures that the interfacial areas quickly increase to the peak preceded by a short initial plateau. Meanwhile, the values of interfacial areas at the λ=2δ box partition are somewhat greater than that of the other three box partitions (λ=4, 6, 8δ); and the results of the other three partitions in all cases demonstrate that there

exists little difference between them. So it is certainly concluded that the maximum stable length scale of drop should be greater than 2δ and less than 4δ. Meanwhile, it is observed that the initial injection temperature of water has significant effect on interfacial area properties as shown above. The higher the initial injection temperature is, the more quickly the total interfacial area is increased with time and the greater its peak value is reached.

Moreover, we also investigated the increasing ratio of interfacial area between liquid water and its surrounding fluid to the assumed undisruptive non-flashing water jet area (its definition is shown in Fig.4-11) as shown in Figs.4-12 and 4-13 for the two choices of the critical Weber number at $\lambda=4\delta$ box partition. The increasing ratio is very useful to roughly estimate the overall SWR rate.

4.4 Conclusions

Based on the direct simulation results of flashing water injection into sodium with the MPS method, the box-counted statistics technique was used to estimate interfacial areas for sodium and liquid water. The effect of initial injection temperature of water on the properties of interfacial area was investigated. It can be concluded as follows:

The initial injection temperature of water has significant effect on the properties of interfacial area. The peak value of the interfacial areas for both sodium and liquid water increases with that temperature, which is due to that the flashing rate at higher initial injection temperature causes more vapor generated and further more intensifies the mixing of sodium, liquid water and vapor. So it is certain that water leak occurring at high temperature position of heat-transfer tubes in steam generators aggravates the

severity of SWR accident.

References

4-1) R-Q. Duan, S. Koshizuka, Y. Oka, T. Takata, and A Yamaguchi, "Direct simulation of flashing liquid injection into liquid by the MPS Method," submitted.

4-2) J. R. Simoes-Moreira, M. M. Vieira, E. Angelo, "Highly expanded flashing liquid jets," *Journal of Thermophysics and Heat Transfer,* 16 415 (2002).

4-3) M. Pilch, C.A. Erdman, "Use of breakup time data and velocity history data to predict the maximum size of stable fragments for acceleration-induced breakup of a liquid drop," Int. *J. Multiphase Flow,* **13**, 741 (1987).

4-4) H. J. Catrakis, R. C. Aguirre, J. Ruiz-Plancarte, "Area-volume properties of fluid interfaces in turbulence: scale-local self-similarity and cumulative scale dependence," *J. Fluid Mech.*, 462, 245 (2002).

4-5) C. H. Lee, R. D.Reitz, "An experimental study of the effect of gas density on the distortion and breakup mechanism of drops in high speed gas stream," *Int. J. Multiphase Flow,* 26, 229 (2000).

4-6) Z. Liu, R. D. Reitz, "An analysis of the distortion and breakup mechanisms of high speed liquid drops," *Int. J. Multiphase Flow,* 23, 631 (1997).

4-7) R. S. Brodkey, *The phenomena of fluid motions*, Addison-Wesley, 552 (1967).

4-8) R-Q. Duan, S. Koshizuka, and Y. Oka, "Two-dimensional simulation of drop deformation and breakup at around the critical Weber number" *Nuclear Engineering and Design*, 225, 37 (2002).

4-9) R-Q. Duan, S. Koshizuka, and Y. Oka, “Numerical and theoretical investigation of effect of density ratio on the critical Weber number of droplet breakup,” *Journal of Nuclear Science and Technology*, 40, 501 (2002).

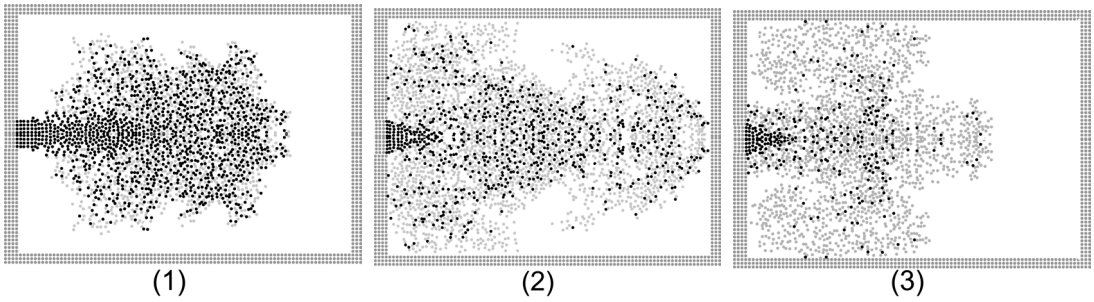

Fig.4-1 Flashing water injection into sodium by direct simulation for different initial injection temperatures by Duan et al. [4-1)]. (1) T=200°C, (2) T=280°C, (3) T=352°C

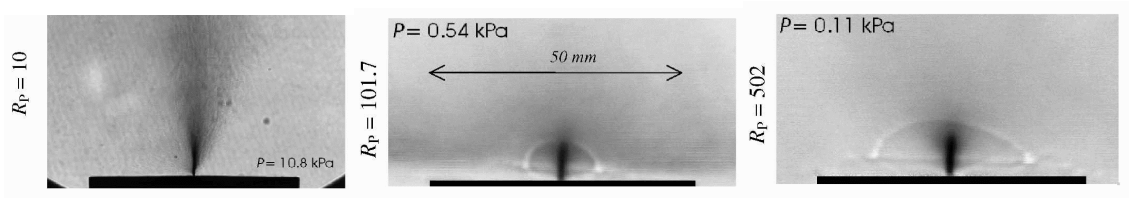

Fig.4-2 The pictures for flashing injection at different pressure depressurization ratio taken by Simoes-Moreira et al. [4-2)].

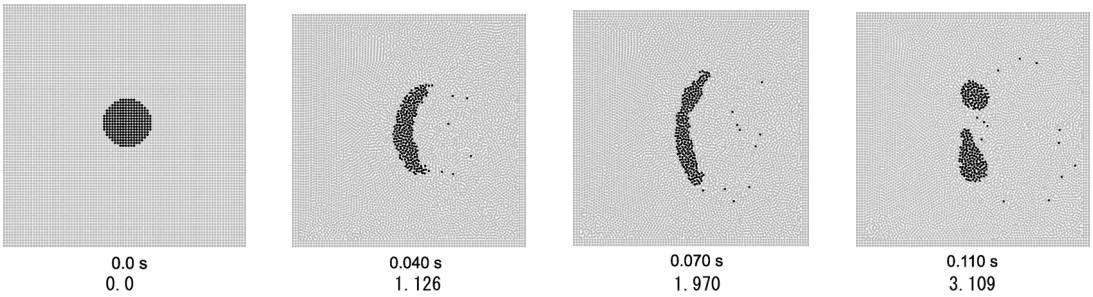

Fig.4-3 Sequence of drop breakup under impulsive acceleration in another liquid at We=13, taken from Duan et al. [4-8)]

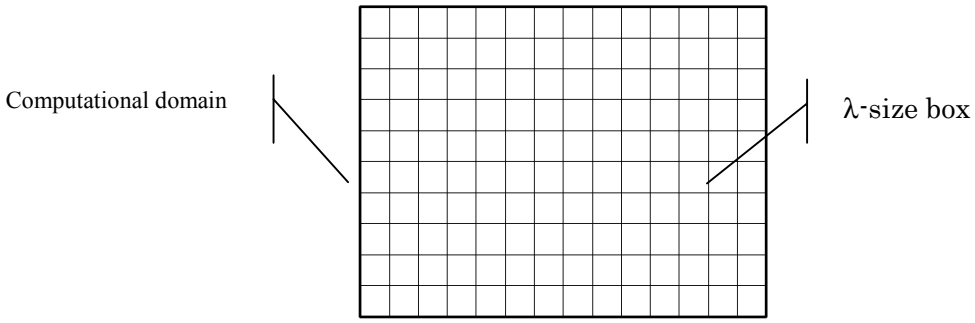

Fig.4-4 Partition of computational domain into λ-size box

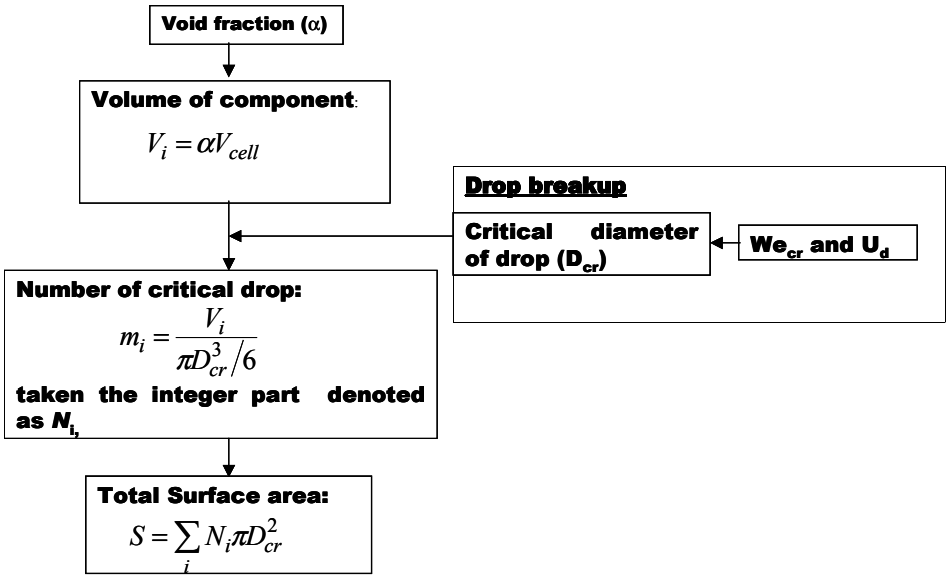

Fig.4-5 Schematic diagram for estimation of interfacial area

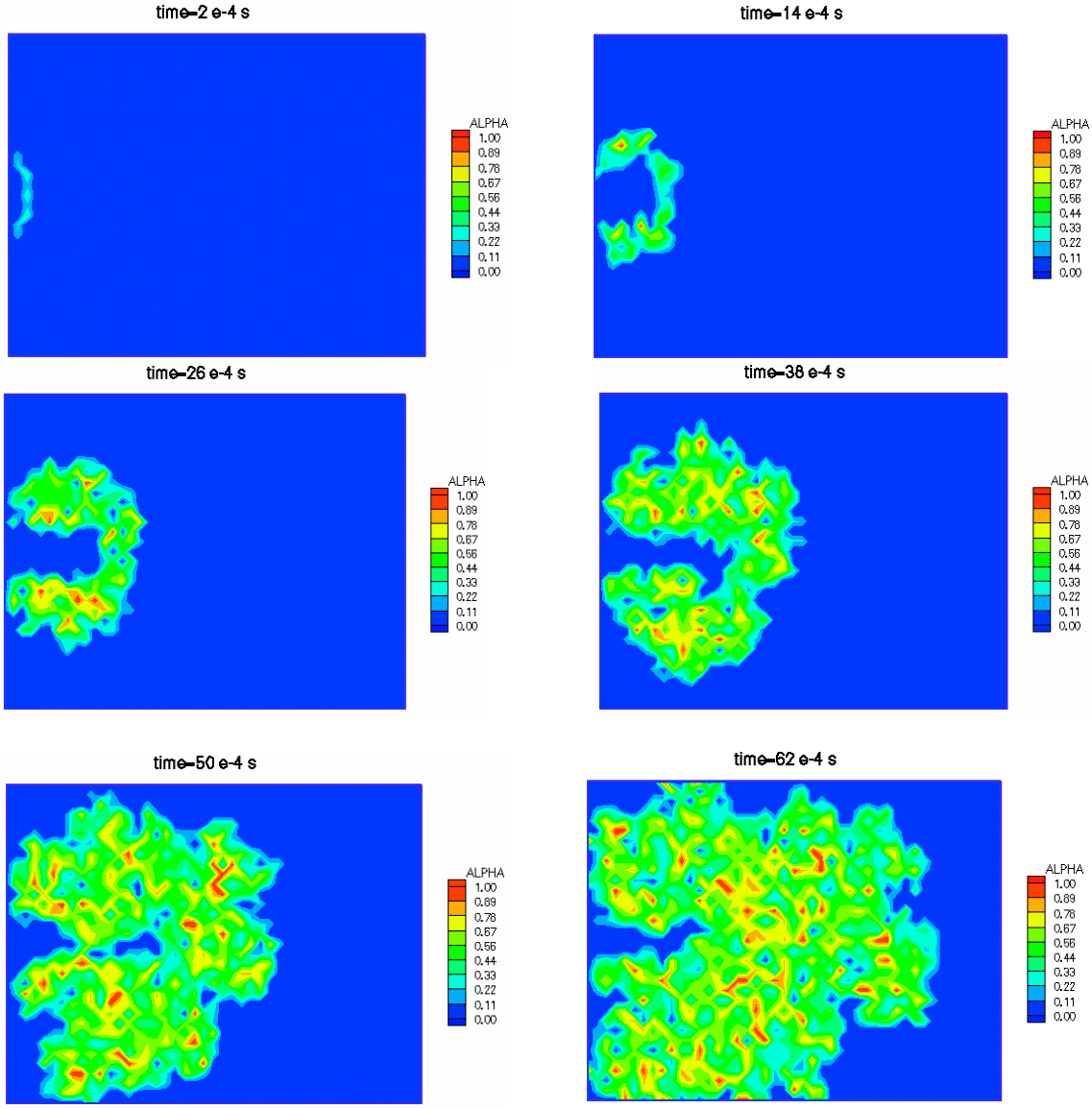

Fig.4-6-a Contour of vapor fraction evolution at initial injection temperature of water T=220°C

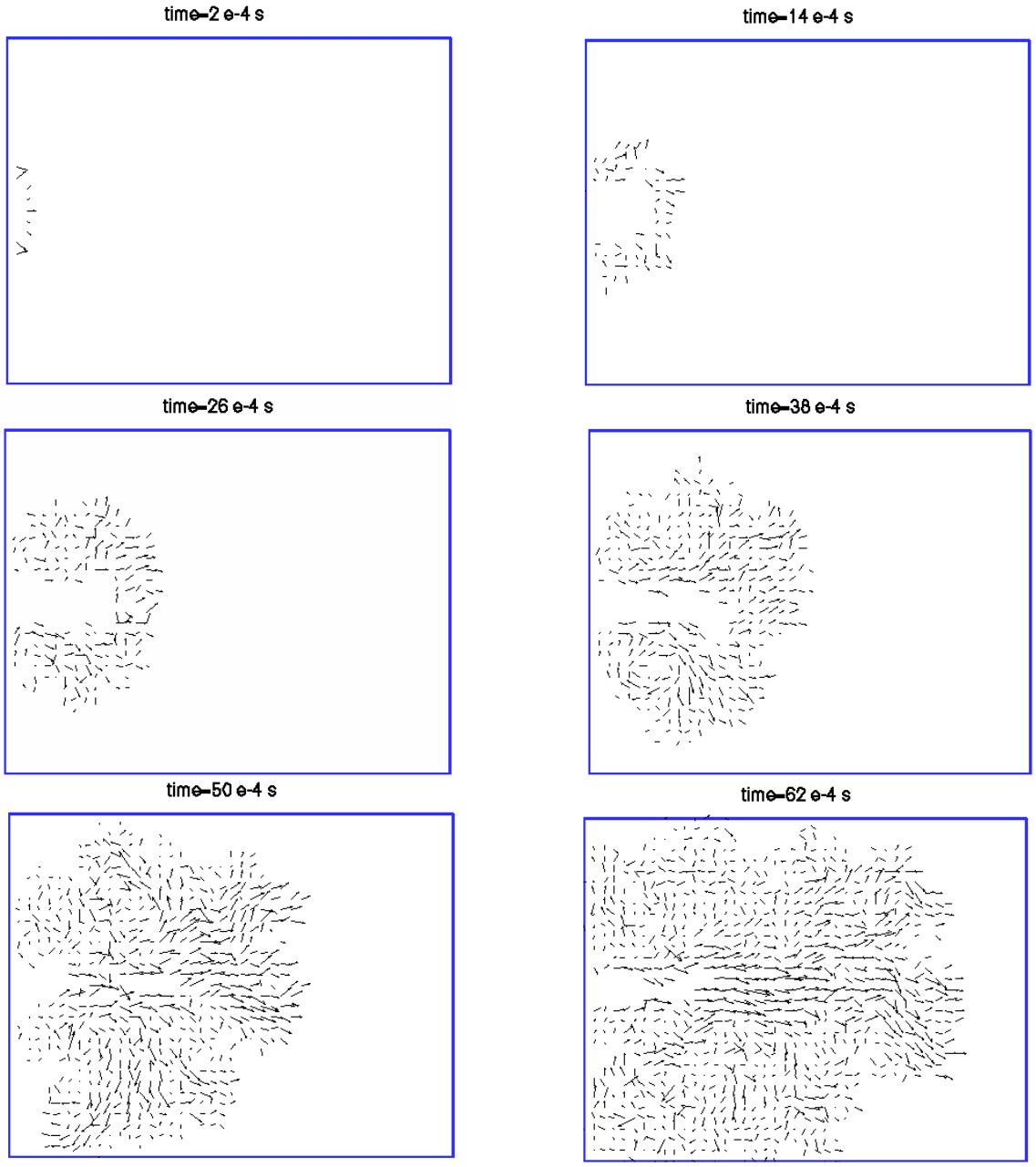

Fig.4-6-b Velocity vector of vapor at initial injection temperature of water T=220°C

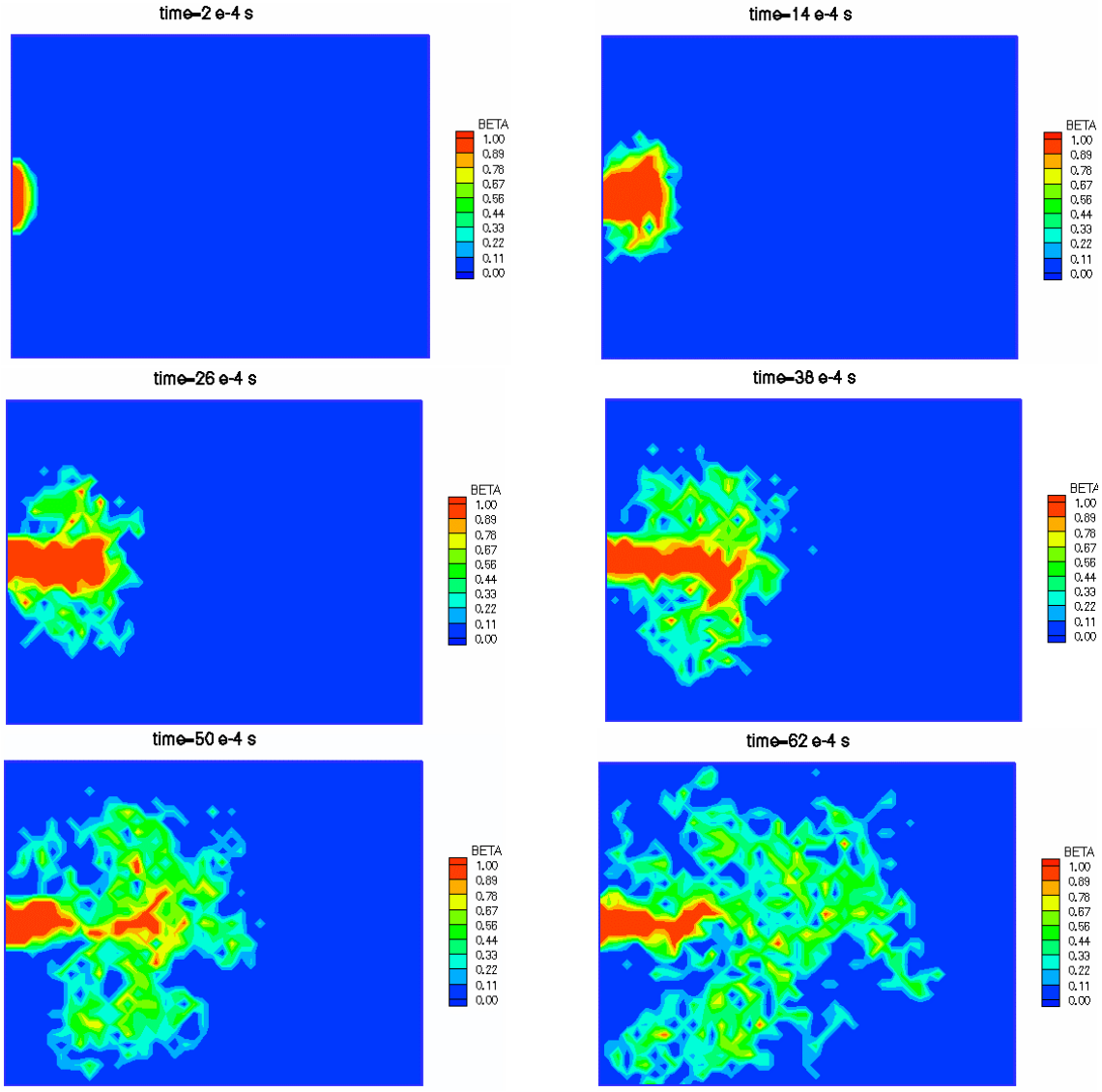

Fig.4-6-c Contour of water fraction evolution at initial injection temperature of water T=220°C

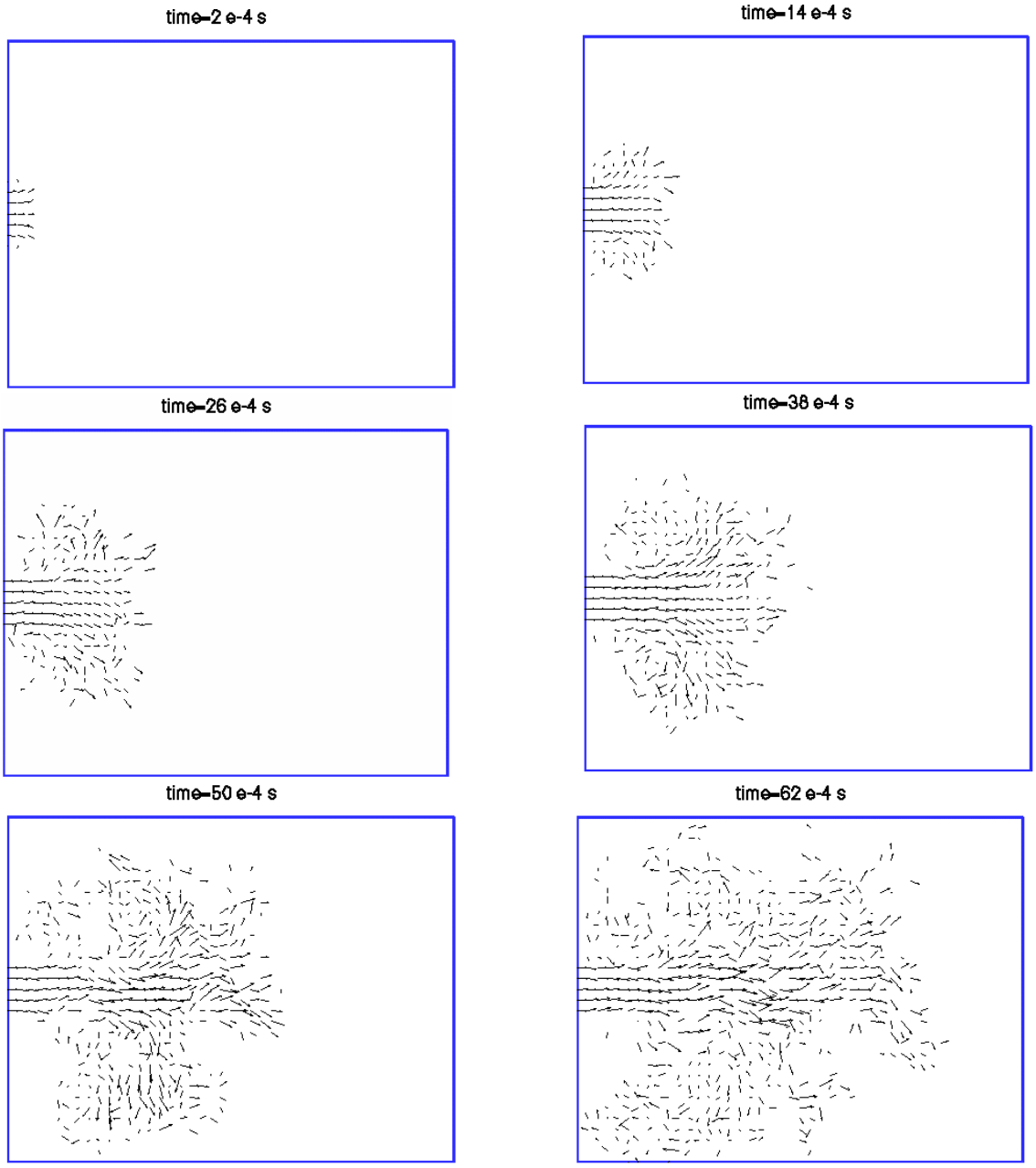

Fig.4-6-d Velocity vector of water at initial injection temperature of water T=220°C

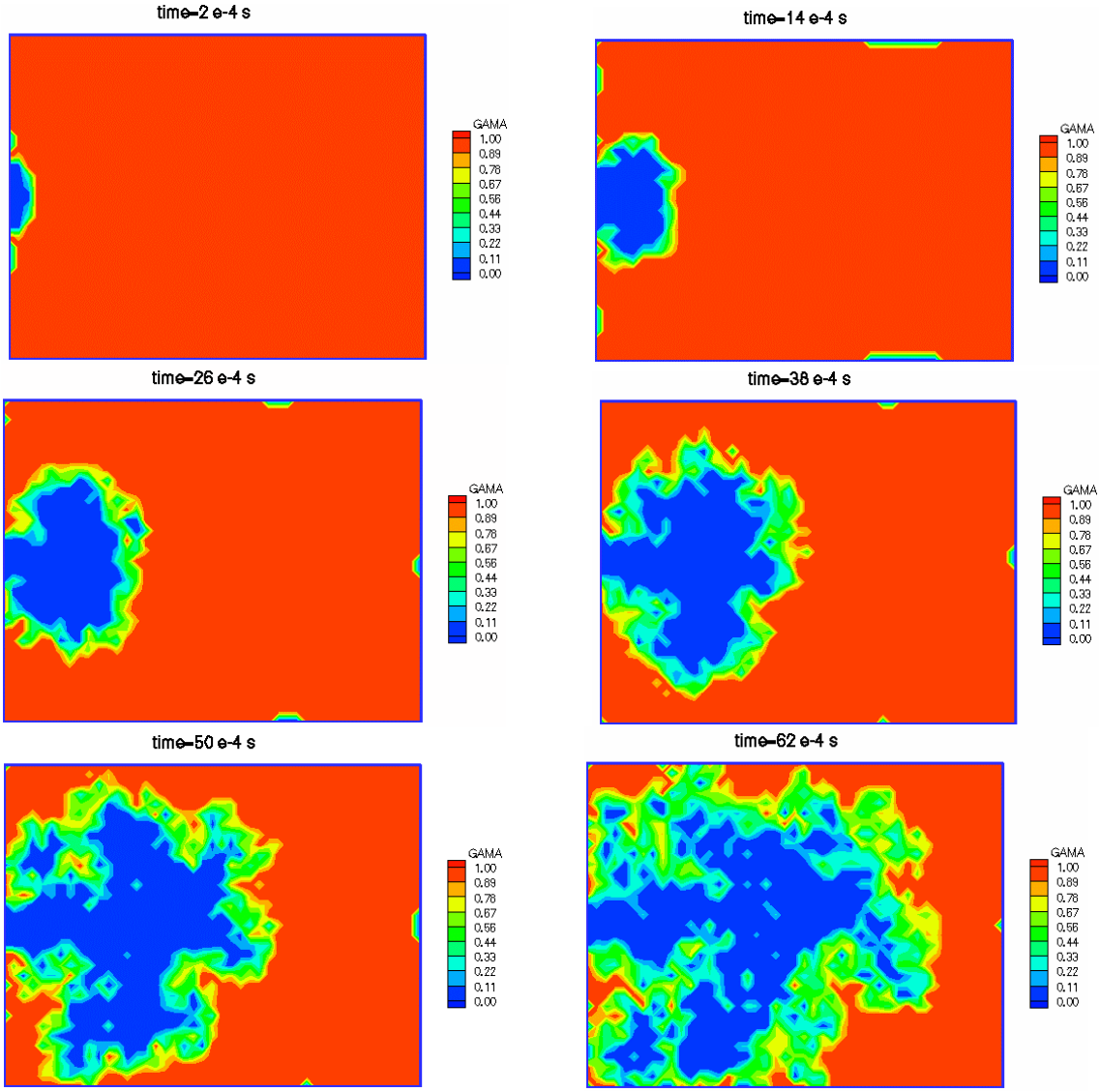

Fig.4-6-e Contour of sodium fraction evolution at initial injection temperature of water T=220°C

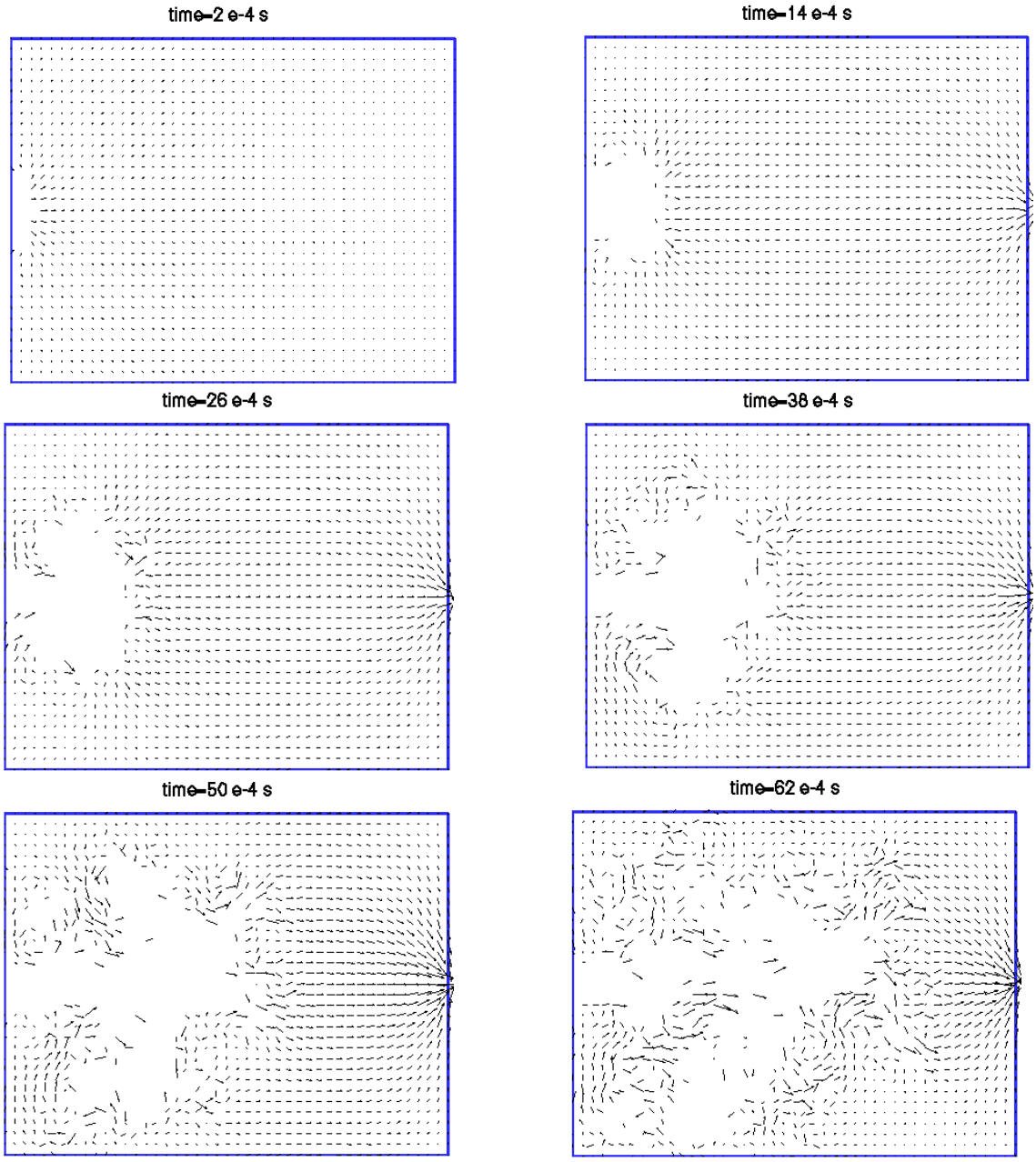

Fig.4-6-f Velocity vector of sodium at initial injection temperature of water T=220°C

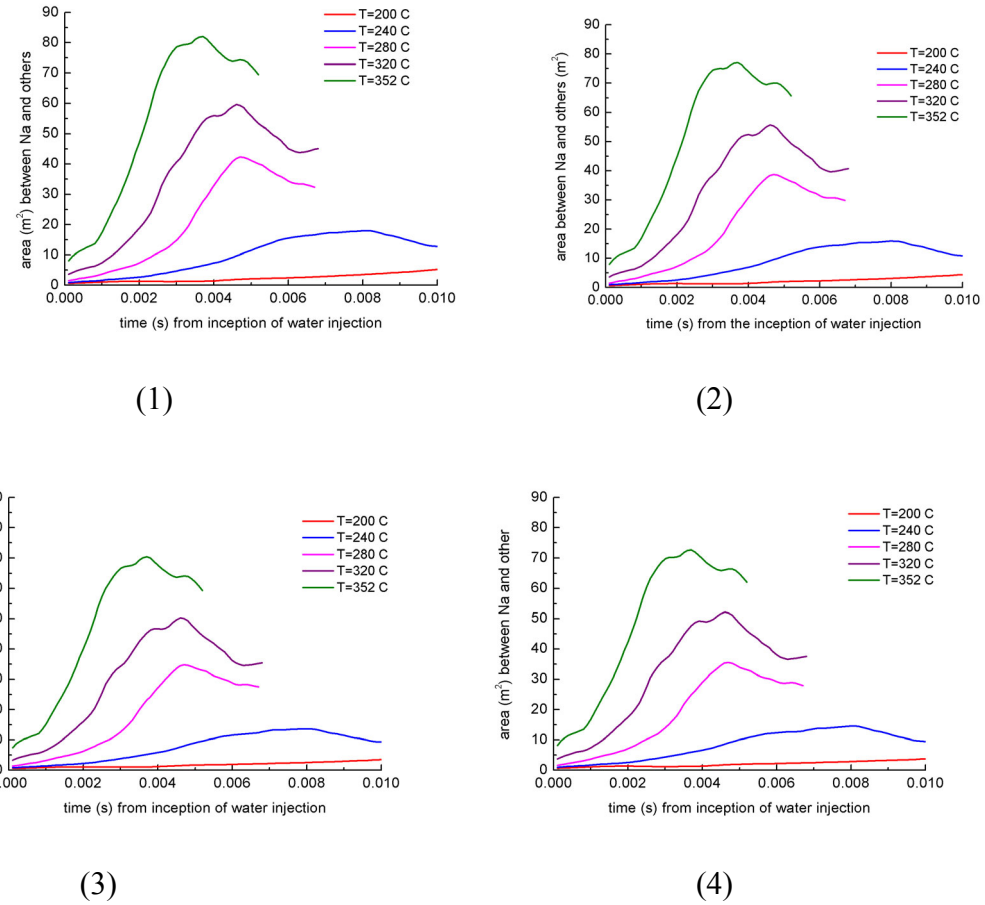

Fig.4-7 Interfacial area between sodium and its surrounding mixture at different initial injection temperatures for We_{cr}=64.36. (1) λ=2×δ box partition, (2) λ=4×δ box partition, (3) λ=6×δ box partition, (4) λ=8×δ box partition

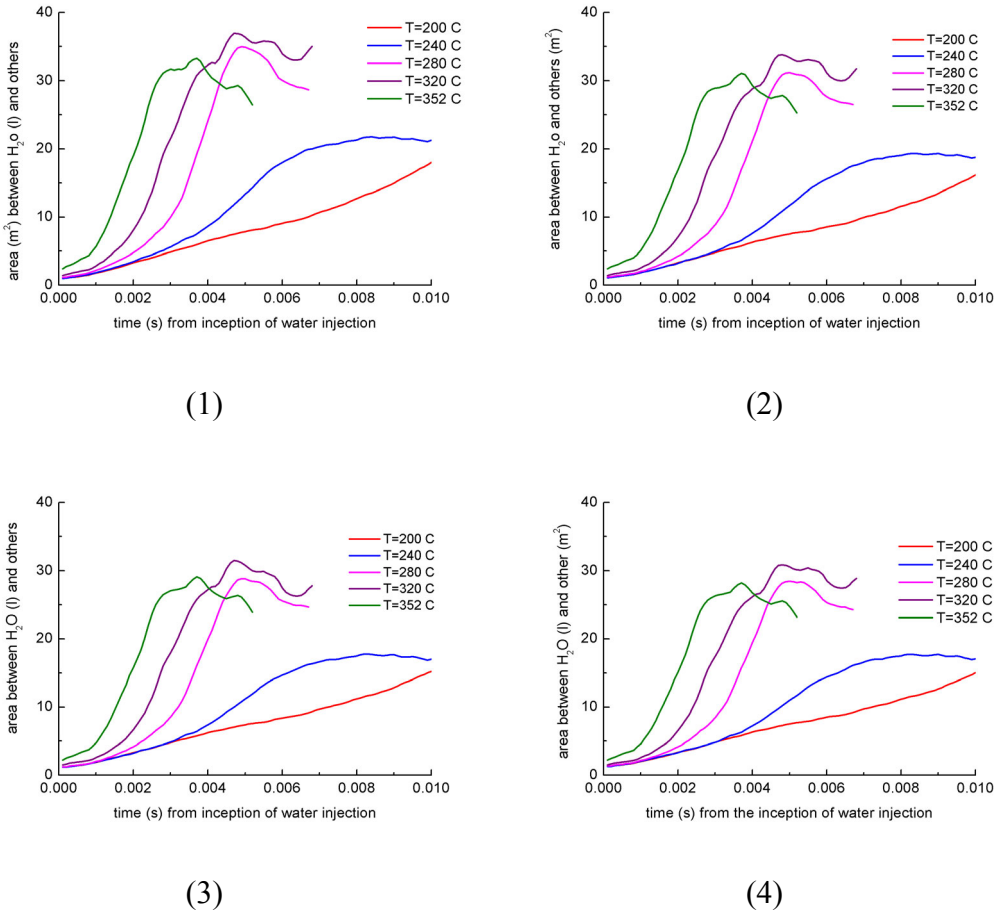

Fig.4-8 Interfacial area between liquid water and its surrounding mixture at different initial injection temperatures for We_{cr}=64.36. (1) λ=2×δ box partition, (2) λ=4×δ box partition, (3) λ=6×δ box partition, (4) λ=8×δ box partition

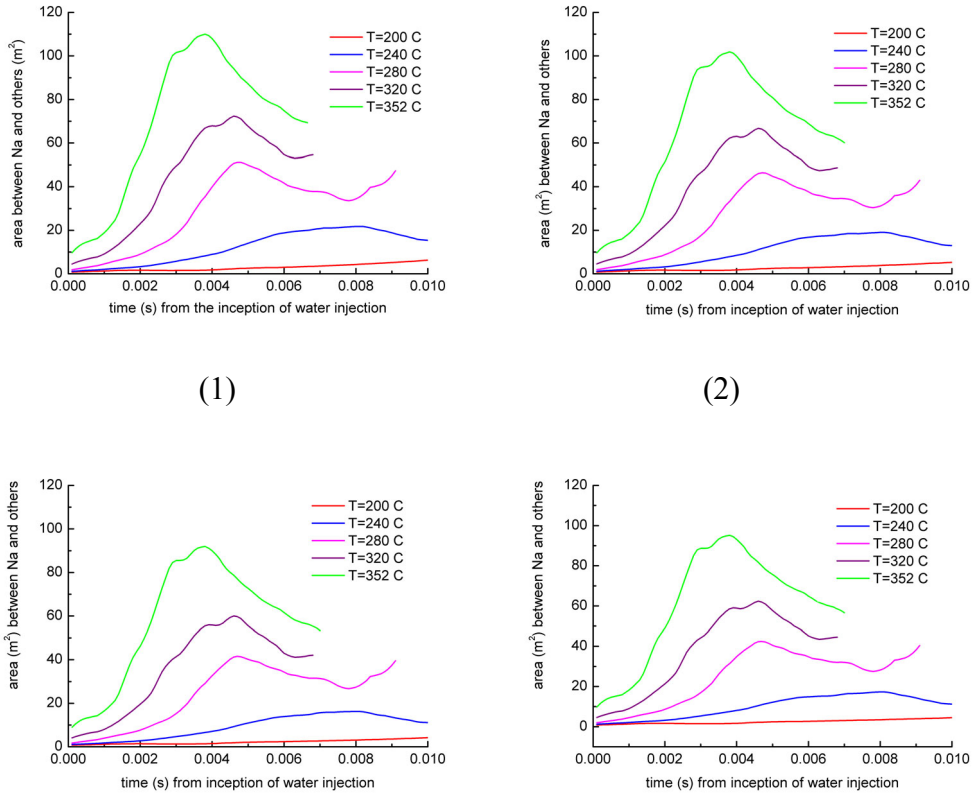

Fig.4-9 Interfacial area between sodium and its surrounding mixture at different initial injection temperatures for $We_{cr} = 64.36(\rho_d / \rho_c)^{-0.82}$. (1) λ=2×δ box partition, (2) λ=4×δ box partition, (3) λ=6×δ box partition, (4) λ=8×δ box partition

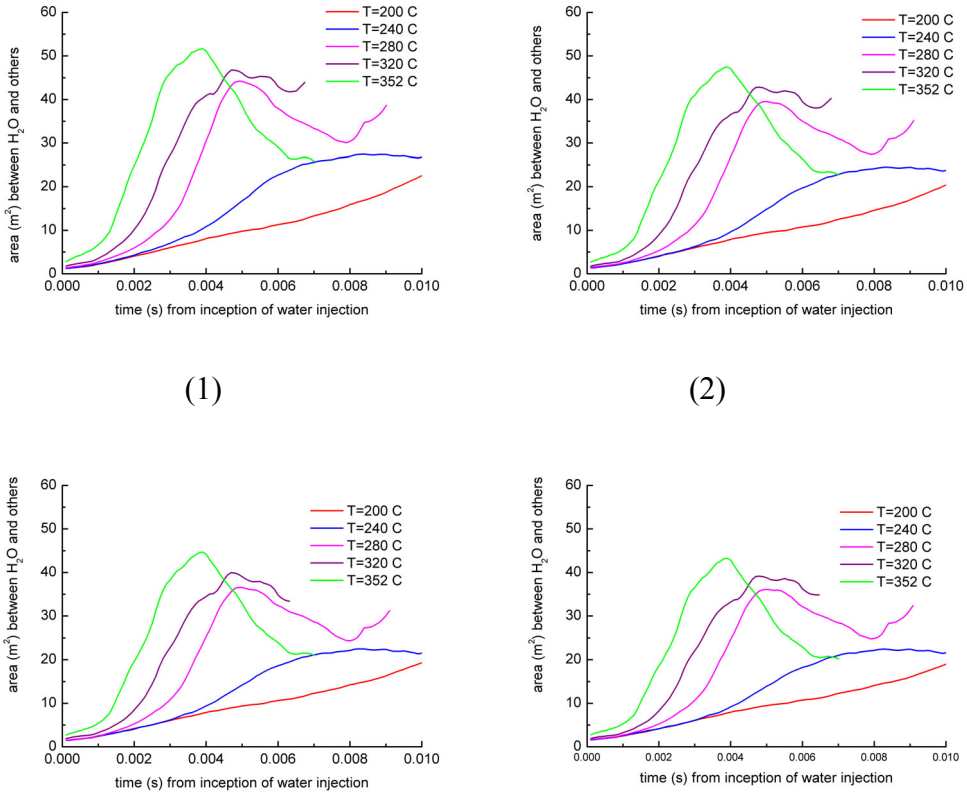

Fig.4-10 Interfacial area between liquid water and its surrounding mixture at different initial injection temperatures for $We_{cr} = 64.36(\rho_d / \rho_c)^{-0.82}$. (1) λ=2×δ box partition, (2) λ=4×δ box partition, (3) λ=6×δ box partition, (4) λ=8×δ box partition

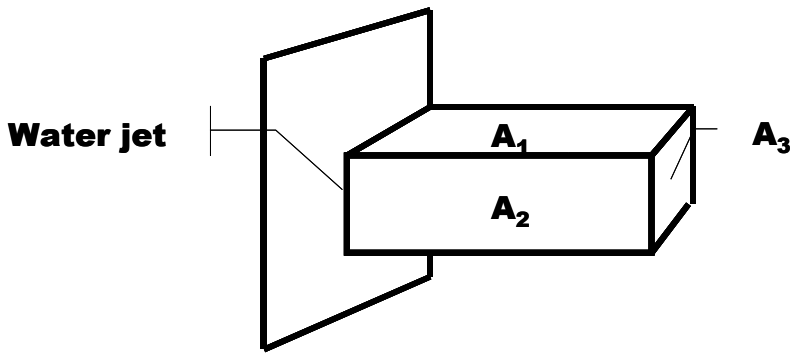

Fig.4-11 Definition of the increasing ratio of interfacial area evolution of water to assumed undisruptive non-flashing water jet area (definition see following Figure, $A=2A_1+2A_2+A_3$)

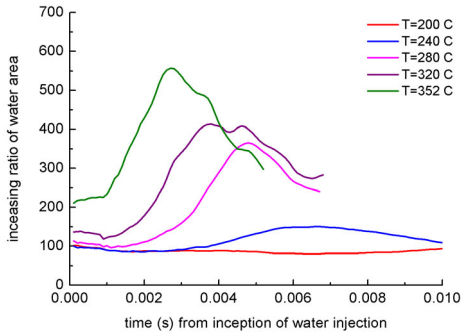

Fig.4-12 The increasing ratio of liquid water area at different initial injection temperatures for We_{cr}=64.36 at λ=4×δ box partition

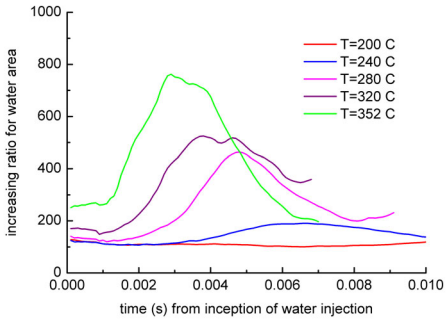

Fig.4-13 The increasing ratio of liquid water area at different initial injection temperatures for $We_{cr} = 64.36(\rho_d/\rho_c)^{-0.82}$ at λ=4×δ box partition

5. Conclusions

Numerical analysis for sodium-water reaction in tube rupture accidents in steam generators in liquid metal-cooled fast breeder reactors (LMFBR) was carried out. A particle method (Moving Particle Semi-implicit, MPS, method) was used to analyze large deformation of interfaces in multi-phase flow.

The effect of density ratio on the critical Weber number has been studied for droplet breakup for liquid-liquid systems by numerical simulations and theoretical analyses. The investigated range of density ratio covers hydrodynamic safety accidents occurred in nuclear reactors. The results show that the critical Weber number is inversely proportional to density ratio; and specifically the critical Weber number is a strong function with density ratio as it is less than 3, but weakly decreased as it is greater than 3. Although there are no complete experimental data to testify this point, our numerical result is consistent with Tan & Bankoff experimental value.

Numerical simulations of flashing liquid injection into liquid were carried out by the MPS method incorporated with the homogeneous non-equilibrium relaxation model. Our numerical simulation results are consistent with Simoes-Moreira *et al.* observations of iso-octane flashing jets: a flashing jet issuing from a nozzle is formed as a central liquid core; the extinction length decreases with increasing injection temperature and tends asymptotically to a constant as the initial injection temperature approaches the saturation temperature corresponding to the injection pressure. The homogeneous two-phase flow is derived which vapor quality increases with increasing the injection initial temperature.

Based on the direct simulation results of the critical Weber number of droplet breakup and water injection into sodium with flashing, the box-counted statistics technique was used to estimate interfacial areas for sodium and liquid water. The initial injection temperature of water has significant effect on the properties of interfacial area. The peak value of the interfacial areas for both sodium and liquid water increases with that temperature, which is due to that the flashing rate at higher initial injection temperature causes more vapor generated and further more intensifies the mixing of sodium, liquid water and vapor. So it is certain that water leak occurring at high temperature position of heat-transfer tubes in steam generators aggravates the severity of sodium-water reaction accidents.

The present study clarified the flow regime in water leakage accidents in steam generators in LMFBR. The interfacial area can be calculated using the mechanistic numerical simulation.